國立臺灣大學理學院大氣科學研究所

碩士論文

Department of Atmospheric Sciences
College of Science
National Taiwan University
Master Thesis

探討海洋大陸在不同砍伐程度下的氣候反應

Exploring Climate Responses to Different Magnitudes of Deforestation in Maritime Continent

李淳弘

Chun-Hung Li

指導教授：羅敏輝 博士

Advisor: Min-Hui Lo, Ph.D.

中華民國 112 年 8 月

August 2023

doi:10.6342/NTU202303778

謝辭

從升大三的暑假透過系上暑期研究的機會開始接觸學術研究，閱讀一些相關的文獻，至此開始進入研究的領域。因為對氣候相關的議題十分感興趣，尤其是人為活動影響氣候的部分，因此當初找了羅敏輝老師討論相關的研究議題。在老師的指導之下，我從研究議題的本質、程式語言的基礎架構開始學起並循序漸進，完成第一份海報並和大家分享研究的成果，也慢慢了解做研究的過程與方法。在上了研究所之後，開始學習全球氣候模式的設定，試著自己跑模式去模擬不同森林砍伐的情境，並探討造成這些現象背後的物理過程與機制。或許現在已經可以談笑風生的打著謝辭，也可以用簡單幾句話和別人描述我的研究動機和想探討的內容，但做研究的過程中並非總是一帆風順，研究所這兩年來處處碰壁是常有的事。有時花了許多時間畫圖，每天晚上離開系館後回想當天的進度卻發現白忙一場，總覺得一大部分變成了沉沒成本;有時因為進度遲滯不前，無形上造成心理壓力也是越來越大。雖然當下面臨這些挫折的時候，仿佛身處黑暗中迷失方向，但自己在研究路上並非孤立無援，很感謝在每週跟羅老師一起討論的時候老師給的建議以及一起腦力激盪的過程，讓我的思緒能夠變清楚並重新回到研究軌道，還願意讓我有機會在畢業前去日本和新加坡進行交流，讓我能夠透過這個機會和大家介紹我的研究，另外要感謝研究室的大家在每學期的 group meeting 提供我許多建議。謝謝小傑學長在跑模式遇到困難時的幫助，謝謝鶴鳴學長教我 ncl 的語法以及 debug，並常常提醒我”太晚了”要早點回家休息，感謝濬濂以及許桀學長陪我一起討論研究，非常感謝大

doi:10.6342/NTU202303778

家的幫忙。

除此之外，想要感謝的人還有很多很多，感謝 B05 的大家，這幾年我們一起吃飯聊天、看棒球、跨年、唱歌等等，讓我的生活除了研究以外還有其他休閒娛樂。謝謝祐軒在我壓力大的時候都願意給我一些建議和鼓勵，還陪我打 Apex，讓我重拾正能量和研究的信心;謝謝吉董在忙於吉氏企業的生意之餘還陪我吃拉麵看棒球以及罵教練團的調度;感謝宇泓、祥任在研究上的幫助也陪我一起爬山，每一次登山都可以把壓力留在山腳下;感謝在遠的要命的瑞士學霸端珩常常跟我視訊聊天聊研究和生活的種種;感謝興泓到學校的時間跟我差不多讓我能夠有早點去學校拍照和認真做研究的動力;感謝俊杰、宇泓、富聖、軒齊、姚博常常一起吃晚餐，在 seminar 和口試前幫我練習和提供建議，在吃飯的時候聽我抱怨讓我紓解壓力，雖然偶爾會說不揪和心結但都還是充滿歡樂。感謝銘豪、俊杰和啟桓陪我打 lol 和 Apex 抒發壓力，儘管我有時一直送頭; 感謝 Jason 常陪我聊天和去玩，每次都能聊好幾個小時，聊天的過程也學到很多，總覺得每次都有所成長;感謝我的高中同學們，尤其是瑋捷和百辰，儘管大學後不在同一間學校，但還是時刻保持聯絡和一起吃飯，在研究所這兩年對我的幫助也很大;還要感謝系壘的大家，系壘就像是第二個家一樣，在球隊從大一待到現在，很喜歡跟大家一起練球和比賽的感覺，每個星期六早上一起練球讓我也能規律的運動。最後要感謝家人無時無刻的支持，讓我無後顧之憂，能盡心盡力地做好眼前應該做好的事情，有了這麼多人在研究上和精神上的支持，我才得以完成這份研究。

doi:10.6342/NTU202303778

摘要

本研究旨在了解在海洋大陸地區不同程度的森林砍伐對氣候的反應，包含平均氣候條件對森林砍伐效應的非線性效應、砍伐後的陸地大氣交互作用變化，以及極端溫度、降水特徵等。本研究主要使用地球系統模式進行了五組不同程度的森林砍伐情境模擬，並額外增加一組砍伐實驗來進行砍伐轉折點的敏感性測試，結果顯示，隨著森林砍伐程度的增加，地表溫度和可感熱通量增加，而潛熱通量則減少。降水也表現出非線性特徵，一開始稍微增加，然後隨著森林砍伐的進行而更明顯地增加。然而，非線性效應可能會因島嶼的分佈和地形而有所不同。舉例來說，婆羅洲地區顯示出一個轉折點，而新幾內亞地區則沒有。在陸地大氣交互作用的部分，本研究使用關鍵土壤濕度和分段回歸的概念探討了森林砍伐後陸地大氣交互作用的變化。結果發現陸地大氣交互作用在砍伐後發生了變化，而土壤濕度回饋可能是導致極端氣溫事件頻率增加重要的角色。

關鍵詞：森林砍伐、海洋大陸地區、非線性效應、陸地大氣交互作用、土壤濕度回饋

doi:10.6342/NTU202303778

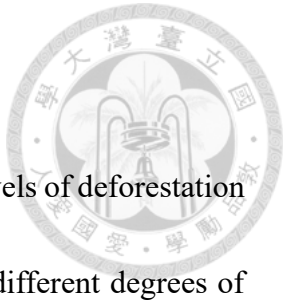

Abstract

This study aims to understand the climate response to varying levels of deforestation in the Maritime Continent (MC), including the nonlinear effects of different degrees of deforestation on average climate conditions, changes in land-atmosphere interactions after deforestation, and the characteristics of extreme temperature and precipitation. Using the Community Earth System Model (CESM), five scenarios of deforestation at different magnitudes were simulated, with an additional sensitivity test to identify the deforestation tipping point. The results show that as deforestation increases, surface temperature and sensible heat flux increase linearly, while latent heat flux decreases linearly. In contrast, precipitation exhibits nonlinear characteristics, initially showing a slight increase and then a more pronounced increase as deforestation progresses. However, the nonlinear effects may vary based on the distribution and terrain of the islands. For instance, a tipping point is observed in the Borneo region, whereas the New Guinea region does not exhibit one. The study explores changes in land-atmosphere interactions after deforestation using the concepts of critical soil moisture and segmented regression. The results indicate that land-atmosphere interactions undergo changes after deforestation, and soil moisture feedback may play a significant role in the increased frequency of extreme temperature events.

Keywords: Deforestation, Maritime Continent, Nonlinear effect, Land atmosphere

doi:10.6342/NTU202303778

interaction, Soil moisture feedback

doi:10.6342/NTU202303778

Contents

doi:10.6342/NTU202303778

doi:10.6342/NTU202303778

Figure Captions

doi:10.6342/NTU202303778

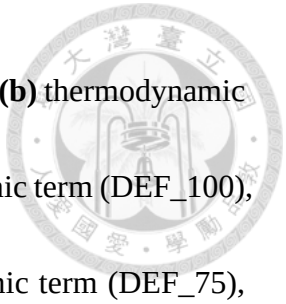

Figure 7. The spatial anomaly of **(a)** thermodynamic term (DEF_25), **(b)** thermodynamic term (DEF_50), **(c)** thermodynamic term (DEF_75), **(d)** thermodynamic term (DEF_100), **(e)** dynamic term (DEF_25), **(f)** dynamic term (DEF_50), **(g)** dynamic term (DEF_75), and **(h)** dynamic term (DEF_100). All plots are compared to CTR_100 and dotted areas indicate p value<0.05.

Figure 8. The spatial anomaly of **(a)** canopy evaporation (DEF_25), **(b)** canopy evaporation (DEF_50), **(c)** canopy evaporation (DEF_75), **(d)** canopy evaporation (DEF_100), **(e)** canopy transpiration (DEF_25), **(f)** canopy transpiration (DEF_50), **(g)** canopy transpiration (DEF_75), **(h)** canopy transpiration (DEF_100), **(i)** soil evaporation (DEF_25), **(j)** soil evaporation (DEF_50), **(k)** soil evaporation (DEF_75), and **(l)** soil evaporation (DEF_100). All are compared to CTR_100 and dots indicate p value<0.05.

Figure 9. The spatial anomaly of **(a)** total runoff (DEF_25), **(b)** total runoff (DEF_50), **(c)** total runoff (DEF_75), **(d)** total runoff (DEF_100), **(e)** surface runoff (DEF_25), **(f)** surface runoff (DEF_50), **(g)** surface runoff (DEF_75), **(h)** surface runoff (DEF_100), **(i)** subsurface runoff (DEF_25), **(j)** subsurface runoff (DEF_50), **(k)** subsurface runoff (DEF_75), **(l)** subsurface runoff (DEF_100), **(m)** infiltration (DEF_25), **(n)** infiltration (DEF_50), **(o)** infiltration (DEF_75), and **(p)** infiltration (DEF_100). All are compared to CTR_100 and dots indicate p value<0.05.

Figure 10. Annual mean **(a)** canopy evaporation, **(b)** canopy transpiration, **(c)** soil

doi:10.6342/NTU202303778

doi:10.6342/NTU202303778

Table Caption

Table1. Model experiments in this study.

doi:10.6342/NTU202303778

1. Introduction

In the past few decades, global forests have undergone rapid changes, especially tropical forests (Hansen et al., 2013; Li et al., 2016). Deforestation can affect local responses in several ways. Firstly, it increases albedo because the albedo of grass or bare ground is higher than that of green trees. Secondly, it reduces evapotranspiration due to land cover changes, which affects latent heat energy and leads to surface warming. Lastly, it reduces surface roughness, which can cause aerodynamic exchanges (Mahmood et al., 2014; Pielke et al., 2016). Such changes in land surface properties can also affect temperature, cloud formation, and precipitation. Additionally, through land-atmospheric processes, modulation of the moisture and energy balance may be further strengthened or weakened depending on the mean state of the region (Koster et al. 2004, Bonan 2008; Seneviratne et al., 2010). For example, if the region falls into an energy-limited regime where soil moisture is sufficient, the atmosphere affects the land through temperature and radiation. Conversely, if the region falls into a water-limited regime where soil moisture is insufficient, the land impacts the atmosphere through evapotranspiration (Seneviratne et al., 2010; Sippel et al., 2017; Tölle et al., 2020). In summary, the climate following deforestation is influenced by changes in energy partition caused by alterations in surface vegetation, as well as the associated land-atmosphere interactions. Overall, deforestation tends to cause an increase in temperature in the tropics and a decrease in high latitudes

doi:10.6342/NTU202303778

(Malyshev et al., 2015; Chen et al., 2020). However, the rising temperatures can cause atmospheric instability, triggering upward motion. Under these circumstances, convergence can bring moisture from the surrounding oceans to the land, competing with the decrease in evapotranspiration (Chen et al., 2019). Therefore, the change in precipitation after deforestation is more complicated than the temperature.

The Maritime Continent (MC), which encompasses some of the world's considerable tropical rainforests, has experienced the highest deforestation rate among the three major tropical rainforest regions, despite receiving less attention (Margono et al., 2012; Gaveau et al., 2014; Stibig et al., 2014; Austin et al., 2017). Located in the tropical region near the equator, the MC region is influenced by monsoon in different seasons. It receives abundant rainfall throughout the year, resulting in consistently high soil moisture levels. These land surface characteristics position it as an energy-limited regime, where evapotranspiration is primarily determined by net radiation (Sippel et al., 2017; Tölle et al., 2020). In recent years, human activities driven by the demand for economic development, which is one of the land use and land cover change (LULCC), have further exacerbated the situation. Extensive deforestation of rainforests in the MC region has become prevalent, often accompanied by the replacement of trees with economically valuable crops such as palm trees (Carlson et al., 2012). These activities, along with large-scale fires caused by lightning strikes or climates, pose significant threats to the region's

doi:10.6342/NTU202303778

ecosystems and biodiversity. The dramatic deforestation alters surface characteristics, affecting energy allocation and the interaction between the atmosphere and the land (Sippel et al., 2017; Vogel et al., 2018). Consequently, LULCC not only disrupts the hydrological cycle (Wohl et al., 2012) but also adjusts the interaction process between the surface and the atmosphere. To address the impacts of deforestation and its consequences on the region, this study will specifically investigate the rainforests of the MC.

Deforestation is an ongoing process that leads to varying climate impacts depending on the extent of deforestation. Different stages of deforestation expose people to different levels of climate risk (Nobre et al., 2016). Gaining a deeper understanding of the potential consequences at different levels of deforestation can greatly assist in implementing proactive measures for mitigation and adaptation to reduce associated risks. Lawrence et al. (2015) discovered that when deforestation is not extensive, continued logging may cause a slight increase in local precipitation until it reaches a tipping point at around 30% in the Amazon region. During this stage, people may not perceive the subtle changes in precipitation resulting from forest alterations. However, if deforestation continues and reaches 70%, a significant decrease in precipitation can be observed compared to areas with no deforestation. At this point, people may experience more frequent droughts, damage to cultivated crops, and disruptions to their livelihoods. This nonlinear impact of deforestation on precipitation exists as a process. Other studies examining varying

doi:10.6342/NTU202303778

degrees of deforestation in the Amazon Basin (Sampaio et al., 2007; Lejeune et al., 2015; Badger et al., 2016) have also identified nonlinear responses of precipitation as deforestation increases. In contrast, previous studies in the MC region have predominantly focused on differences after complete deforestation (Werth and Avissar, 2005; Chen et al., 2019; Tölle et al., 2017). Despite the availability of ensemble data on different levels of global deforestation from the Land Use Model Intercomparison Project (Lawrence et al., 2016), the analysis of this dataset revealed no significant changes in temperature and precipitation in the MC region (Li et al., 2022). This could be attributed to the insufficient extent of deforested area, interannual variability, and the regulating influence of the surrounding ocean, making it challenging to quantify the impact of deforestation on the climate in the MC region. Therefore, we aim to investigate the rainforest region surrounded by the ocean through an ideal deforestation experiment. Our main objective is to determine whether a nonlinear relationship exists between different levels of deforestation and climate impacts, such as patterns in the hydrological cycle. Additionally, we seek to examine how land-atmosphere interactions before and after deforestation influence both the mean climate state and extreme events. By comprehending the consequences of severe deforestation in this region, we can make informed decisions to mitigate its effects.

doi:10.6342/NTU202303778

2. Methodology

2.1 Model Description and Simulation Setup

To explore the nonlinearities in climate responses under different magnitudes of deforestation in the MC region, an idealized experiment was conducted using Community Earth System Model (Hurrell et al., 2013). Five simulations were mainly performed: CTR_100 (all trees), DEF_25 (25% deforested), DEF_50 (50% deforested), DEF_75 (75% deforested), and DEF_100 (all deforested), with an additional sensitivity test, DEF_35 (35% deforested), to explore the deforestation tipping point. The simulations encompassed monthly and daily data over a 60-year period, with the initial 5 years dedicated to spin-up. The forest distribution is illustrated in Figure 1, and more detailed information about the model experiments is provided in Table 1.

The simulations were conducted using the "F_2000_CAM5" configuration, with a horizontal resolution of 0.9° x 1.25° and 30 vertical levels. This configuration couples the Community Atmosphere Model (CAM) with CAM5 physics (Neale et al., 2012) to the Community Land Model version 4 (CLM4.0; Lawrence et al., 2011). Climatological sea surface temperatures averaged from 1982 to 2001 were prescribed in the model. In the CTR_100 case, all plant functional types in the MC region (between 11°S–11°N and 90°–150°E) were replaced with broadleaf evergreen tropical trees, representing an idealized non-deforested condition that hypothesizes the absence of urbanization and

doi:10.6342/NTU202303778

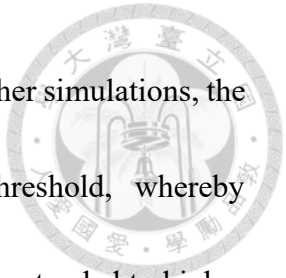

industrialization in the original environment a long time ago. In the other simulations, the deforestation areas were determined by using altitude as a threshold, whereby deforestation began from low-level regions such as coastal areas and extended to higher regions such as mountains, where broadleaf evergreen tropical trees were replaced with C4 grass. The spatial distributions of these simulations resemble real-world deforestation patterns (Stibig et al., 2014; Crompton et al., 2021). The calculation of the deforested ratio can be determined by using the proportion of grassland area to the forest area of CTR_100.

2.2 Moist Static Energy

If there is higher energy in the lower atmosphere, it tends to create an unstable environment that potentially leads to upward motion, favoring the development of convection. To understand how atmospheric stability changes with increasing deforestation magnitude, we analyze the moist static energy (MSE), which is composed of sensible, latent, and potential energy:

$$\mathrm{MSE} = \mathrm{C_p T} + \mathrm{Lq} + \mathrm{gz} \quad (1)$$

In equation (1), Cp represents the specific heat at constant pressure for air, T denotes temperature, L is the latent heat of vaporization, q represents specific humidity, g represents the acceleration of gravity, and z represents height.

2.3 Moisture Budget Analysis

doi:10.6342/NTU202303778

To understand the mechanisms underlying changes in precipitation following deforestation, we further employed the integrated moisture budget equation for analysis:

$$P' \approx ET' - \langle v \cdot \nabla q \rangle' - \left\langle \omega \frac{\partial q}{\partial p} \right\rangle' \quad (2)$$

In equation (2), the prime symbol (') indicates the anomaly between the control case and deforestation cases. P represents precipitation, ET denotes evapotranspiration, $\langle v \cdot \nabla q \rangle$ represents vertically integrated horizontal moisture advection, and $\left\langle \omega \frac{\partial q}{\partial p} \right\rangle$ represents integrated vertical moisture advection. The latter can be divided into two components: the thermodynamic and dynamic terms, which are calculated as follows:

$$-\left\langle \omega \frac{\partial q}{\partial p} \right\rangle' \approx -\left\langle \bar{\omega} \frac{\partial q'}{\partial p} \right\rangle - \left\langle \omega' \frac{\partial \bar{q}}{\partial p} \right\rangle \quad (3)$$

In equation (3), the bar sign denotes the value of the control simulation, that is, CTR_100, and the unit used in the water budget equations is W/m^2.

2.4 Critical Soil Moisture and Changes in Land-Atmosphere Interaction

To examine the land-atmosphere interaction before and after deforestation, we utilized the segmented regression method (Muggeo et al., 2008; Schwingshackl et al., 2017; Hsu et al., 2022) to determine the critical soil moisture (CSM) values. By plotting the relationship between soil moisture and latent heat flux, we observed two critical soil moisture thresholds. The first threshold separates soil moisture into transitional and wet regimes, as observed in regions like Central America. The second threshold distinguishes between wet and very wet regimes. In our study, we focused on analyzing the land-

doi:10.6342/NTU202303778

atmosphere interactions in the MC region, which is located in an energy-limited area. This region falls under the latter case mentioned earlier. Within the MC region, when the soil moisture is not sufficiently wet, we observed no significant correlation between soil moisture and latent heat flux. Conversely, when the soil moisture reaches extremely high levels, a negative relationship between the two variables emerges, primarily due to reduced net radiation (Hsu et al., 2022). Therefore, we believe that the effects of land-atmosphere interactions differ in these two scenarios and require separate investigations. By employing CSM, we aim to enhance our understanding of surface energy partitioning (Feldman et al., 2019; Denissen et al., 2020) within the MC region. This distinctive characteristic of the MC region motivated us to conduct further research on land-atmosphere interactions in this specific area. Consistent with previous studies (Denissen et al., 2020; Tölle et al., 2020), we employed correlation coefficients to analyze changes in land-atmosphere interaction. We conducted correlation and regression analyses for pairs of soil moisture (SM), maximum temperature (TSMX), radiative flux absorbed at the surface (SR), and latent heat flux (LH). This analysis utilized monthly data spanning a period of 660 months, with a specific focus on the differences between CTR_100 and DEF_100, allowing us to explore the impact of deforestation on land-atmosphere interactions in the MC region.

2.5 Statistical Analysis

doi:10.6342/NTU202303778

To assess whether significant differences exist in climate responses after different degrees of deforestation in the MC region, we utilized a two-tailed Student's t-test for statistical hypothesis testing at a significance level of 95% (based on 660 months of data).

To analyze extreme events, we employed daily data and plotted probability density functions to examine changes in climate variables, such as maximum temperature (TSMX), minimum temperature (TSMN), average temperature (TS), and precipitation (PRECT).

doi:10.6342/NTU202303778

3. Results

3.1 Atmospheric Response

3.1.1 Spatial Characteristics

Figures 2a to 2d depict the area anomalies of latent heat flux, while Figures 2e to 2h depict that of sensible heat flux. Due to the change in plant types from broadleaf evergreen tropical trees to C4 grass, there is a reduction in evapotranspiration and surface roughness in the deforested region, leading to a decrease in latent heat flux. However, the sensible heat flux increases due to the repartition effect. Additionally, slight responses are also observed in some non-forested regions after deforestation (e.g., the latent heat flux in coastal regions and the sensible heat flux in some inland areas), which may be due to changes in the wind field. Figures 3a to 3d show that temperature increases in the deforested areas, dominated by the local effect. In contrast, precipitation shows different behavior compared to the other three variables, with changes relatively concentrated in the deforested areas. At low levels of deforestation (DEF_25), precipitation slightly increases, but in some regions such as Sumatra and Borneo, there is even a slight decrease, although it is not statistically significant. As the deforested area increases, precipitation starts to increase more, and we can see that until the total area is deforested, almost every region on land shows a significant increase in precipitation, as shown in Figures 3e to 3h. This phenomenon indicates that in addition to local changes, other factors may also affect

doi:10.6342/NTU202303778

precipitation.

3.1.2 Nonlinearities

Spatial averaging reveals that latent heat flux decreases (as shown in Figure 4a), while both sensible heat flux and surface temperature increase with the intensity of deforestation (as depicted in Figure 4b and Figure 4c). The response of these three climate variables to deforestation is rather linear, primarily influenced by local effects. In contrast, precipitation exhibits nonlinear behavior. It is evident that precipitation in non-deforested areas also undergoes changes, and the increase in precipitation is not uniformly distributed. In summary, precipitation shows a slight increase at low levels of deforestation (DEF_25), followed by a more substantial increase as deforestation progresses (as illustrated in Figure 4d).

3.1.3 Qualitative Analysis

To explain the nonlinearity of the increase in precipitation, we initially focus on the stability of the vertical structure of the atmosphere. We analyze this by examining the MSE and investigating the changes in stability under varying degrees of deforestation. Figures 5a to 5d depict the MSE anomalies over the land relative to the control run. In the case of DEF_25, there are minimal changes in sensible heat, latent heat, and potential energy. Conversely, as the extent of deforestation increases, there is a rise in sensible heat and a decline in latent heat flux near the surface. Furthermore, we observe an

doi:10.6342/NTU202303778

augmentation in the latent heat term at the low levels, primarily associated with the occurrence of deforestation-induced low-level water vapor convergence when the deforested area reaches a significant size. With further progression of deforestation, the expansive deforested area heats the surface, causing air parcels to ascend even higher. As air is a continuous fluid, it needs to be replenished from surrounding areas. In this scenario, the air is sourced from the ocean, carrying more water vapor onto the land. Consequently, we find that water vapor begins to accumulate over the land, and almost every region in the MC region experiences a substantial increase in water vapor until complete deforestation occurs (as depicted in Figure 6). Under these circumstances, there is an increase in energy compared to CTR_100, and the heightened water vapor content may lead to increased rainfall when the atmospheric conditions are unstable.

3.1.4 Quantitative Analysis

While qualitative analysis can help us understand the possible causes of increased precipitation, it does not allow us to determine the dominant factor. To analyze the main factors contributing to increased precipitation, we apply the moisture budget equation. Among these factors, integrated vertical moisture advection have been found to play a more significant role compared to evapotranspiration and integrated horizontal moisture advection after deforestation. Therefore, we present the results specifically for vertical term across different degrees of deforestation. Figures 7a to 7d depict the thermodynamic

doi:10.6342/NTU202303778

term while Figures 7e to 7h depict dynamic term for various deforestation scenarios. As the degree of deforestation increases, the contribution of the thermodynamic term becomes increasingly negative, although not significantly so. Conversely, the dynamic term exhibits a positive contribution, albeit not initially obvious, with some areas even showing a slight negative contribution at the beginning (DEF_25). However, as the degree of deforestation intensifies, the positive contribution of the dynamic term becomes much more pronounced, several times larger than that of the thermodynamic term. Consequently, the dynamic term dominates the changes in precipitation in the MC region.

3.2 Land Response

3.2.1 Spatial Characteristics

In the previous section, we discussed the impacts of deforestation on temperature, precipitation, and latent and sensible heat flux. In this section, our main focus will be on investigating evapotranspiration and runoff. Changes in plant types, in addition to temperature and precipitation, can also affect the overall evapotranspiration process. After deforestation, both canopy evaporation and transpiration decrease due to the presence of fewer leaves in C4 grass compared to tropical broadleaf trees. The reduced leaf area intercepts less water, and the fewer stomata result in weaker evapotranspiration (Figures 8a to 8h). Conversely, as the degree of deforestation intensifies, more precipitation reaches the ground, leading to increased soil evaporation (Figures 8i to 8l). However, this

doi:10.6342/NTU202303778

increase is insufficient to compensate for the reduced canopy evapotranspiration.

As is known, deforestation intensifies, affecting both precipitation and evapotranspiration, consequently impacting the amount of runoff. Figure 9 illustrate the area anomalies related to total runoff, surface runoff, subsurface runoff, and infiltration. Typically, runoff is strongly influenced by precipitation. When precipitation reaches the ground surface, it fills depression storage, and a portion of the water infiltrates to replenish groundwater, while the rest becomes surface runoff. Figures 9a to 9d demonstrate a highly positive correlation between the spatial distribution of total runoff and land precipitation. Figures 9e to 9l reveal that changes induced by deforestation primarily stem from an increase in subsurface runoff. As for infiltration, when the extent of deforestation increases, some regions experience an increase, such as the inland of Borneo when the degree of deforestation is large enough (DEF_75 and DEF_100), as well as the New Guinea region, and the increase reaches its maximum in DEF_100. Meanwhile, coastal regions tend to decrease in all cases, as shown in Figures 9m to 9p.

3.2.2 Nonlinearities

We further perform spatial averaging on canopy evaporation, transpiration, soil evaporation, runoff, and infiltration to discuss their characteristics. The analysis reveals that both canopy evaporation and canopy transpiration decrease as the extent of deforestation expands (Figure 10a and Figure 10b). In contrast, soil evaporation increases

doi:10.6342/NTU202303778

with the magnitude of deforestation (Figure 10c). Regarding runoff, as the extent of forest logging continues to increase, there is a consistent trend of an increased volume of runoff, whether for subsurface or surface runoff (Figures 10d to 10f). Furthermore, compared to precipitation, the increase in runoff is even greater, nearly twice as much. This indicates that changes in runoff appear to be more sensitive than changes in precipitation. Consequently, the increase in precipitation caused by deforestation could potentially result in severe flooding in the area. As for infiltration, it shows another condition, which only increases in the case of DEF_100 and is dominated by the contribution of the New Guinea region (Figure 10g).

3.3 Hydrological Cycle

The hydrological cycle encompasses evaporation, transpiration, condensation, precipitation, and runoff. Based on the previous analysis, it is evident that deforestation has an impact on temperature and precipitation patterns. Changes in the land surface also influence evapotranspiration and runoff, thereby modifying the entire hydrological cycle during the deforestation process. In section 3.3, our main focus is to provide an explanation for the observed increase in runoff.

In experiments conducted at different levels of deforestation, we plotted the probability distribution of total water storage (TWS) for all months after subtracting the average of CTR_100 (Figure 11). It was found that as the degree of deforestation

doi:10.6342/NTU202303778

increased, the annual variability of changes in soil moisture content appeared to decrease. One possible explanation is that when the TWS is high, the soil moisture content may approach saturation. If the soil is already saturated, most of the rainfall on the land will become runoff. The MC region is originally a moist and rainy area, and we have observed that deforestation in the MC region leads to increased precipitation, making it easier for the soil moisture to reach saturation. Additionally, the reduction in evapotranspiration makes the region more dependent on runoff to remove excess rainfall.

3.4 Land Atmosphere Interaction

The introduction section mentions that alterations in surface vegetation can lead to changes in energy partitioning, potentially affecting the strength of land-atmosphere interactions. To simplify the land-atmospheric interaction after deforestation, we only examine the cases of CTR_100 and DEF_100. Before determining the CSM in the MC region, it is crucial to consider whether deforestation causes a shift in the CSM, as this could impact the selection of thresholds. As a result, we found that the CSM is around 0.32 in both CTR_100 and DEF_100 by using segmented regression. Due to the existence of some uncertainties (or errors) in the estimation, we use two thresholds, soil moisture less than 0.3 and greater than 0.35, as the criteria for different mean states. After applying segmented regression to identify the CSM and categorizing the mean state of soil moisture, we can further examine the coupling strength between land and atmosphere under

doi:10.6342/NTU202303778

different categories after deforestation.

After conducting correlation and regression analyses for pairs of soil moisture, maximum temperature, radiative flux absorbed at the surface, and latent heat flux, we found that some of them exhibit distinct characteristics. Consequently, we selected those variables for further discussion. Figures 12a and 12b depict a scatter plot showing the relationship between soil moisture and latent heat flux. A notable characteristic observed from this plot is that the relationship between soil moisture and latent heat flux differs between wet conditions (represented by red dots) and extremely wet conditions (represented by blue dots), both before and after deforestation. Figures 12c and 12d illustrate the relationship between soil moisture and maximum temperature. It is evident that after deforestation, the overall coupling strength (negative correlation) becomes stronger for wet soil moisture conditions. Furthermore, change of the slope also suggests that soil moisture has become more responsive to changes in maximum temperature with an increase in the variability of maximum temperature after complete deforestation. These changes can be attributed to the enhancement of the soil moisture-temperature feedback mechanism (Seneviratne et al., 2010; Vogel et al., 2018). As soil moisture decreases, evapotranspiration reduces, leading to a warmer atmosphere, which, in turn, further depletes soil moisture, creating a positive feedback loop. Additionally, as mentioned earlier, changes in land-atmosphere interactions and energy allocation result in an

doi:10.6342/NTU202303778

increase in surface temperature after deforestation. These alterations contribute to the overall temperature rise and an increase in the annual temperature range. Figures 12e and 12f depict the coupling strength between maximum temperature and latent heat flux. In contrast to the relationship between soil moisture and maximum temperature, the coupling between latent heat flux and maximum temperature weakens after deforestation.

3.5 Extreme Cases

So far, we have focused on examining changes in climate conditions concerning the mean state. However, it is crucial to consider the impact of deforestation on extreme values as they can have a greater influence on natural disasters. For instance, extremely high temperatures increase the frequency of heatwaves, and in severe cases, even wildfires. Similarly, intense precipitation can result in flooding, especially in low-lying areas. Therefore, in addition to studying the effects of deforestation on average climate conditions, it is equally important to investigate how extreme events will be altered.

3.5.1 Temperature

Figures 13a to 13c depict the probability distribution of daily mean surface temperature (TS), daily maximum temperature (TSMX), and daily minimum temperature (TSMN) on land. Our findings indicate that as deforestation increases, there is a slight increase in both TS and TSMN, while TSMX exhibits the most significant increase. In general, the distribution of TS and TSMN shows greater similarity compared to the

doi:10.6342/NTU202303778

distribution of TS and TSMX. To summarize, we observed a nonlinear increase in the frequency of high temperatures for TSMX, accompanied by an increase in temperature variability. The fact that the increase in the frequency of TSMX is larger than TSMN after deforestation can be attributed to two main factors. Firstly, the stronger daytime radiation intensity results in higher values for variables such as sensible heat and radiation compared to nighttime, leading to a more pronounced impact on daytime temperatures. Secondly, changes in land-atmosphere interactions, particularly the soil moisture-temperature feedback mechanism discussed in the previous section, contribute to a significant increase in the frequency of extremely high temperatures. In previous studies, the phenomenon of increased temperature variability following deforestation has been observed as well (Alkama and Cescatti, 2016; Schultz et al., 2017; McAlpine et al., 2018; Chapman et al., 2020).

3.5.2 Precipitation

For mean precipitation on land, as depicted in Figure 13d, the frequency of light rain and heavy rain increases, while the frequency of moderate rain decreases as the deforestation area expands. After deforestation, there appears to be a phenomenon of "rich get richer, poor get poorer." The most significant increase in average precipitation occurs in the complete deforestation case. However, the underlying mechanism for these changes is still unknown that deserves a further study.

doi:10.6342/NTU202303778

4. Conclusion and Discussion

This study utilizes the CESM model to investigate the impact of varying levels of deforestation on the climate of the MC region. Our analysis focuses on understanding the nonlinear changes occurring in both the atmosphere and land as a result of deforestation. We also explore variations in the hydrological cycle and examine how soil moisture influences land-atmosphere interactions. Additionally, we analyze the effects of deforestation on extreme temperature and precipitation patterns.

Our results reveal that linear changes in temperature, latent heat flux, and sensible heat flux are primarily influenced by local conditions, while precipitation does not exhibit a linear trend. In contrast to the findings of Lawrence et al. (2015), precipitation shows a slight initial increase followed by further increases as the deforested area expands. This behavior may be associated with atmospheric stability and water transport. Further analysis using MSE and wind convergence suggests that the increase in precipitation may be linked to changes in atmospheric stability and low-level atmospheric water vapor transport. The moisture budget equation allows us to quantify the dominant factor causing the changes in precipitation and indicates that the dynamic term plays a significant role in the observed increase in rainfall. However, nonlinearities in precipitation trends may also be influenced by terrain and the distribution of deforestation. In the case of Borneo, when the percentage of deforestation is small, precipitation slightly decreases, but as the

doi:10.6342/NTU202303778

deforested area increases, precipitation starts to increase, indicating a tipping point (Figure 14a). In contrast, for New Guinea, precipitation slightly increases at low levels of deforestation, and it continues to increase as the deforested area expands. The absence of a tipping point in New Guinea is observed (Figure 14b). Regarding total evapotranspiration, our findings indicate that canopy evaporation and transpiration decrease, while soil evaporation increases due to more rain falling directly onto the ground and less transpiration. In terms of runoff, we observe that as the degree of deforestation increases, the increase in runoff is approximately twice the amount of precipitation. This observed increase in runoff can be attributed to a combination of increased precipitation following deforestation and changes in vegetation, which make the soil layer more susceptible to saturation. These alterations significantly impact the hydrological cycle. Deforestation changes the land surface properties as well as atmospheric condition, which modify land-atmosphere interactions through energy redistribution, resulting in distinct responses observed in different mean states of soil moisture. This is particularly evident in the soil moisture- temperature feedback mechanism, which influences extreme temperature events and likely contributes to the significant increase in high temperatures following deforestation. However, the mechanisms underlying the increase in light and heavy rainfall after deforestation remain unknown.

doi:10.6342/NTU202303778

Based on our research, we speculate that the decrease in evapotranspiration resulting from deforestation and the subsequent low-level atmospheric moisture convergence is associated with changes in precipitation patterns. However, due to the limited number of experimental groups in our study, which included only five different deforestation levels, it is challenging to conclusively determine whether a tipping point exists for the MC region. To address this uncertainty, we conducted an additional experiment, DEF_35, to explore the nonlinear behavior of precipitation. The results revealed that precipitation is even higher in this case compared to the DEF_25 experiment (Figure 14c). This trend is observed even in regions like Sumatra and Borneo, where precipitation initially shows a slight decrease. These findings suggest that in our study, convergence may start to dominate the changes in precipitation when the deforestation percentage exceeds 25%. If a tipping point exists in our study, it is likely to occur when the deforested proportion is below 25%, where the low-level water vapor convergence still not obvious. Compared to the real world, Wei et al. (2022) revealed that the Indonesian forest disappeared with the forest extent dropping from 124.5 Mha in 1980 to 91.0 Mha in 2015 (approximately 20%), while the precipitation shows an increasing trend using the data from the Global Precipitation Climatology Centre (GPCC). However, it is worth mentioning that both satellite observation data and different models have their uncertainties. For instance, precipitation results differ among the Global Precipitation Climatology Project (GPCP),

doi:10.6342/NTU202303778

GPCC, and ERA5 datasets. Furthermore, some studies utilizing different models have found that rainfall tends to decrease after deforestation (Tölle et al., 2017; Chapman et al., 2020), which differs from our results. Although the change in precipitation might also be affected by model uncertainties, interannual variability such as ENSO or by the effect of global warming, it is also crucial to note from our study that if deforestation of rainforests is not mitigated, it could potentially accelerate the increase in precipitation and have a greater impact on runoff, increasing the risk of severe flooding in the future.

Another interesting observation is that both our study and the study by Chen et al. (2019) indicate that the dynamic term is the main factor driving changes in precipitation. However, in the scenario of global warming, it seems that the thermodynamic term dominates the intensity and increase of precipitation (Chou et al.,2012). In the real world, global warming and deforestation often occur concurrently. Therefore, it can be expected that the extent of temperature rise would be even greater, while the influence of precipitation could become more complex. Nevertheless, it remains essential for us to actively engage in mitigation and adaptation measures to minimize risks and address the potential impacts of these changes.

doi:10.6342/NTU202303778

References

Alkama, R., & Cescatti, A. (2016). Biophysical climate impacts of recent changes in global forest cover. *Science*, *351*(6273), 600-604. https://doi.org/10.1126/science.aac8083

Austin, K. G., González-Roglich, M., Schaffer-Smith, D., Schwantes, A. M., & Swenson, J. J. (2017). Trends in size of tropical deforestation events signal increasing dominance of industrial-scale drivers. *Environmental Research Letters*, *12*(5), 054009. https://doi.org/10.1088/1748-9326/aa6a88

Badger, A. M., & Dirmeyer, P. A. (2016). Diagnosing nonlinearities in the local and remote responses to partial Amazon deforestation. *Journal of Geophysical Research: Atmospheres*, *121*(15), 9033-9047. https://doi.org/10.1002/2015JD024013

Bonan, G. B. (2008). Forests and climate change: forcings, feedbacks, and the climate benefits of forests. *Science*, *320*(5882), 1444-1449. https://doi.org/10.1126/science.1155121

Carlson, K. M., Curran, L. M., Ratnasari, D., Pittman, A. M., Soares-Filho, B. S., Asner, G. P., Trigg, S. N., Gaveau, D. A., Lawrence, D., & Rodrigues, H. O. (2012). Committed carbon emissions, deforestation, and community land conversion from oil palm plantation expansion in West Kalimantan, Indonesia. *Proceedings of the National Academy of Sciences*, *109*(19), 7559-7564.

doi:10.6342/NTU202303778

https://doi.org/10.1073/pnas.1200452109

Chapman, S., Syktus, J., Trancoso, R., Salazar, A., Thatcher, M., Watson, J. E. M., Meijaard, E., Sheil, D., Dargusch, P., & McAlpine, C. A. (2020). Compounding impact of deforestation on Borneo's climate during El Niño events. *Environmental Research Letters*, *15*(8), 084006. https://doi.org/10.1088/1748-9326/ab86f5

Chen, C.-C., Lo, M.-H., Im, E.-S., Yu, J.-Y., Liang, Y.-C., Chen, W.-T., Tang, I., Lan, C.-W., Wu, R.-J., & Chien, R.-Y. (2019). Thermodynamic and Dynamic Responses to Deforestation in the Maritime Continent: A Modeling Study. *Journal of Climate*, *32*(12), 3505-3527. https://doi.org/10.1175/JCLI-D-18-0310.1

Chen, L., & Dirmeyer, P. A. (2020). Reconciling the disagreement between observed and simulated temperature responses to deforestation. *Nature Communications, 11*(1), 202. https://doi.org/10.1038/s41467-019-14017-0

Chou, C., Chen, C.-A., Tan, P.-H., & Chen, K. T. (2012). Mechanisms for Global Warming Impacts on Precipitation Frequency and Intensity. *Journal of Climate*, *25*(9), 3291-3306. https://doi.org/10.1175/JCLI-D-11-00239.1

Crompton, O., Corrêa, D., Duncan, J., & Thompson, S. (2021). Deforestation-induced surface warming is influenced by the fragmentation and spatial extent of forest loss in Maritime Southeast Asia. *Environmental Research Letters*, *16*. https://doi.org/10.1088/1748-9326/ac2fdc

doi:10.6342/NTU202303778

Denissen, J. M. C., Teuling, A. J., Reichstein, M., & Orth, R. (2020). Critical Soil Moisture Derived From Satellite Observations Over Europe. *Journal of Geophysical Research: Atmospheres*, *125*(6), e2019JD031672. https://doi.org/10.1029/2019JD031672

Feldman, A. F., Short Gianotti, D. J., Trigo, I. F., Salvucci, G. D., & Entekhabi, D. (2019). Satellite-Based Assessment of Land Surface Energy Partitioning–Soil Moisture Relationships and Effects of Confounding Variables. *Water Resources Research*, *55*(12), 10657-10677. https://doi.org/10.1029/2019WR025874

Gaveau, D. L. A., Sloan, S., Molidena, E., Yaen, H., Sheil, D., Abram, N. K., Ancrenaz, M., Nasi, R., Quinones, M., Wielaard, N., & Meijaard, E. (2014). Four Decades of Forest Persistence, Clearance and Logging on Borneo. *PLoS One*, *9*(7), e101654. https://doi.org/10.1371/journal.pone.0101654

Hansen, M. C., Potapov, P. V., Moore, R., Hancher, M., Turubanova, S. A., Tyukavina, A., Thau, D., Stehman, S. V., Goetz, S. J., Loveland, T. R., Kommareddy, A., Egorov, A., Chini, L., Justice, C. O., & Townshend, J. R. G. (2013). High-Resolution Global Maps of 21st-Century Forest Cover Change. *Science*, *342*(6160), 850-853. https://doi.org/10.1126/science.1244693

Hsu, H., & Dirmeyer, P. A. (2022). Deconstructing the Soil Moisture–Latent Heat Flux Relationship: The Range of Coupling Regimes Experienced and the Presence of

doi:10.6342/NTU202303778

Nonlinearity within the Sensitive Regime. *Journal of Hydrometeorology*, *23*(7), 1041-1057. https://doi.org/10.1175/JHM-D-21-0224.1

Hurrell, J. W., Holland, M. M., Gent, P. R., Ghan, S., Kay, J. E., Kushner, P. J., Lamarque, J., Large, W. G., Lawrence, D., Lindsay, K., Lipscomb, W. H., Long, M. C., Mahowald, N., Marsh, D. R., Neale, R. B., Rasch, P., Vavrus, S., Vertenstein, M., Bader, D., Collins, W. D., Hack, J. J., Kiehl, J., & Marshall, S. (2013). The Community Earth System Model: A Framework for Collaborative Research. *Bulletin of the American Meteorological Society*, *94*(9), 1339-1360. https://doi.org/10.1175/BAMS-D-12-00121.1

Koster, R. D., Dirmeyer, P. A., Guo, Z., Bonan, G., Chan, E., Cox, P., Gordon, C. T., Kanae, S., Kowalczyk, E., Lawrence, D., Liu, P., Lu, C.-H., Malyshev, S., McAvaney, B., Mitchell, K., Mocko, D., Oki, T., Oleson, K., Pitman, A., . . . Yamada, T. (2004). Regions of Strong Coupling Between Soil Moisture and Precipitation. *Science*, *305*(5687), 1138-1140. https://doi.org/10.1126/science.1100217

Lawrence, D. M., Oleson, K. W., Flanner, M. G., Thornton, P. E., Swenson, S. C., Lawrence, P. J., Zeng, X., Yang, Z.-L., Levis, S., Sakaguchi, K., Bonan, G. B., & Slater, A. G. (2011). Parameterization improvements and functional and structural advances in Version 4 of the Community Land Model. *Journal of Advances in Modeling Earth Systems*, *3*(1). https://doi.org/10.1029/2011MS00045

doi:10.6342/NTU202303778

Lawrence, D., & Vandecar, K. (2015). Effects of tropical deforestation on climate and agriculture. *Nature Climate Change*, *5*(1), 27-36. https://doi.org/10.1038/nclimate2430

Lawrence, D. M., Hurtt, G. C., Arneth, A., Brovkin, V., Calvin, K. V., Jones, A. D., Jones, C. D., Lawrence, P. J., de Noblet-Ducoudré, N., Pongratz, J., Seneviratne, S. I., & Shevliakova, E. (2016). The Land Use Model Intercomparison Project (LUMIP) contribution to CMIP6: rationale and experimental design. *Geosci. Model Dev.*, *9*(9), 2973-2998. https://doi.org/10.5194/gmd-9-2973-2016

Lejeune, Q., Davin, E. L., Guillod, B. P., & Seneviratne, S. I. (2015). Influence of Amazonian deforestation on the future evolution of regional surface fluxes, circulation, surface temperature and precipitation. *Climate Dynamics*, *44*(9), 2769-2786. https://doi.org/10.1007/s00382-014-2203-8

Li, Y., Zhao, M., Mildrexler, D. J., Motesharrei, S., Mu, Q., Kalnay, E., Zhao, F., Li, S., & Wang, K. (2016). Potential and Actual impacts of deforestation and afforestation on land surface temperature. *Journal of Geophysical Research: Atmospheres*, *121*(24), 14,372-314,386. https://doi.org/10.1002/2016JD024969

Li, Y., Brando, P. M., Morton, D. C., Lawrence, D. M., Yang, H., & Randerson, J. T. (2022). Deforestation-induced climate change reduces carbon storage in remaining tropical forests. *Nature Communications*, *13*(1), 1964.

doi:10.6342/NTU202303778

https://doi.org/10.1038/s41467-022-29601-0

Mahmood, R., Pielke Sr., R. A., Hubbard, K. G., Niyogi, D., Dirmeyer, P. A., McAlpine, C., Carleton, A. M., Hale, R., Gameda, S., Beltrán-Przekurat, A., Baker, B., McNider, R., Legates, D. R., Shepherd, M., Du, J., Blanken, P. D., Frauenfeld, O. W., Nair, U. S., & Fall, S. (2014). Land cover changes and their biogeophysical effects on climate. *International Journal of Climatology*, *34*(4), 929-953. https://doi.org/10.1002/joc.3736

Malyshev, S., Shevliakova, E., Stouffer, R. J., & Pacala, S. W. (2015). Contrasting Local versus Regional Effects of Land-Use-Change-Induced Heterogeneity on Historical Climate: Analysis with the GFDL Earth System Model. *Journal of Climate*, *28*(13), 5448-5469. https://doi.org/10.1175/JCLI-D-14-00586.1

Margono, B. A., Turubanova, S., Zhuravleva, I., Potapov, P., Tyukavina, A., Baccini, A., Goetz, S., & Hansen, M. C. (2012). Mapping and monitoring deforestation and forest degradation in Sumatra (Indonesia) using Landsat time series data sets from 1990 to 2010. *Environmental Research Letters*, *7*(3), 034010. https://doi.org/10.1088/1748-9326/7/3/034010

McAlpine, C. A., Johnson, A., Salazar, A., Syktus, J., Wilson, K., Meijaard, E., Seabrook, L., Dargusch, P., Nordin, H., & Sheil, D. (2018). Forest loss and Borneo's climate. *Environmental Research Letters*, *13*(4), 044009. https://doi.org/10.1088/1748-

doi:10.6342/NTU202303778

9326/aaa4ff

Muggeo, V. (2008). Segmented: An R Package to Fit Regression Models With Broken-Line Relationships. *R News*, *8*, 20-25.

Neale, R. B., and Coauthors, 2012: Description of the NCAR Community Atmosphere Model (CAM 5.0). NCAR Tech. Note NCAR/TN-4861STR, 274 pp., www2.cesm.ucar.edu/models/cesm1.0/cam/docs/description/cam5_desc.pdf.

Nobre, C., Sampaio, G., Borma, L., Castilla-Rubio, J., Silva, J., & Cardoso, M. (2016). Land-use and climate change risks in the Amazon and the need of a novel sustainable development paradigm. *Proceedings of the National Academy of Sciences of the United States of America*, *113*. https://doi.org/10.1073/pnas.1605516113

Pielke, R. A., Sr, Mahmood, R., & McAlpine, C. (2016). Land's complex role in climate change. *Physics Today*, *69*(11), 40-46. https://doi.org/10.1063/pt.3.3364

Sampaio, G., Nobre, C., Costa, M. H., Satyamurty, P., Soares-Filho, B. S., & Cardoso, M. (2007). Regional climate change over eastern Amazonia caused by pasture and soybean cropland expansion. *Geophysical Research Letters*, *34*(17). https://doi.org/10.1029/2007GL030612

Schultz, N. M., Lawrence, P. J., & Lee, X. (2017). Global satellite data highlights the diurnal asymmetry of the surface temperature response to deforestation. *Journal of Geophysical Research: Biogeosciences*, *122*(4), 903-917.

doi:10.6342/NTU202303778

https://doi.org/10.1002/2016JG003653

Schwingshackl, C., Hirschi, M., & Seneviratne, S. (2017). Quantifying Spatiotemporal Variations of Soil Moisture Control on Surface Energy Balance and Near-Surface Air Temperature. *Journal of Climate*, *30*. https://doi.org/10.1175/JCLI-D-16-0727.1

Seneviratne, S. I., Corti, T., Davin, E. L., Hirschi, M., Jaeger, E. B., Lehner, I., Orlowsky, B., & Teuling, A. J. (2010). Investigating soil moisture–climate interactions in a changing climate: A review. *Earth-Science Reviews*, *99*(3), 125-161. https://doi.org/10.1016/j.earscirev.2010.02.004

Sippel, S., Zscheischler, J., Mahecha, M. D., Orth, R., Reichstein, M., Vogel, M., & Seneviratne, S. I. (2017). Refining multi-model projections of temperature extremes by evaluation against land–atmosphere coupling diagnostics. *Earth Syst. Dynam.*, *8*(2), 387-403. https://doi.org/10.5194/esd-8-387-2017

Stibig, H. J., Achard, F., Carboni, S., Raši, R., & Miettinen, J. (2014). Change in tropical forest cover of Southeast Asia from 1990 to 2010. *Biogeosciences*, *11*(2), 247-258. https://doi.org/10.5194/bg-11-247-2014

Tölle, M. H., Engler, S., & Panitz, H.-J. (2017). Impact of Abrupt Land Cover Changes by Tropical Deforestation on Southeast Asian Climate and Agriculture. *Journal of Climate*, *30*(7), 2587-2600. https://doi.org/10.1175/JCLI-D-16-0131.1

Tölle, M. H. (2020). Impact of Deforestation on Land–Atmosphere Coupling Strength

doi:10.6342/NTU202303778

and Climate in Southeast Asia. *Sustainability*, *12*(15), 6140. https://doi.org/10.3390/su12156140

Vogel, M. M., Zscheischler, J., & Seneviratne, S. I. (2018). Varying soil moisture–atmosphere feedbacks explain divergent temperature extremes and precipitation projections in central Europe. *Earth Syst. Dynam.*, *9*(3), 1107-1125. https://doi.org/10.5194/esd-9-1107-2018

Wei, S., Wang, X., & Xie, Q. (2023). Strengthening effect of Maritime Continent deforestation on the precipitation decline over southern China during late winter and early spring. *Climate Dynamics*, *60*(3), 1173-1185. https://doi.org/10.1007/s00382-022-06362-6

Werth, D., & Avissar, R. (2005). The local and global effects of Southeast Asian deforestation. *Geophysical Research Letters*, *32*(20). https://doi.org/10.1029/2005GL022970

Wohl, E., Barros, A., Brunsell, N., Chappell, N. A., Coe, M., Giambelluca, T., Goldsmith, S., Harmon, R., Hendrickx, J. M. H., Juvik, J., McDonnell, J., & Ogden, F. (2012). The hydrology of the humid tropics. Nature Climate Change, 2(9), 655-662. https://doi.org/10.1038/nclimate1556

doi:10.6342/NTU202303778

Table

Table1. Model information in this study

Experiments	Description
CTR_100	All are broadleaf evergreen tropical trees
DEF_25	25% of the total area is deforested and replaced by C4 grasses
DEF_35	35% of the total area is deforested and replaced by C4 grasses
DEF_50	50% of the total area is deforested and replaced by C4 grasses
DEF_75	75% of the total area is deforested and replaced by C4 grasses
DEF_100	All are C4 grasses
Time	All cases run 60 years with monthly and daily data, and first five years used for spin up time.

doi:10.6342/NTU202303778

Figures

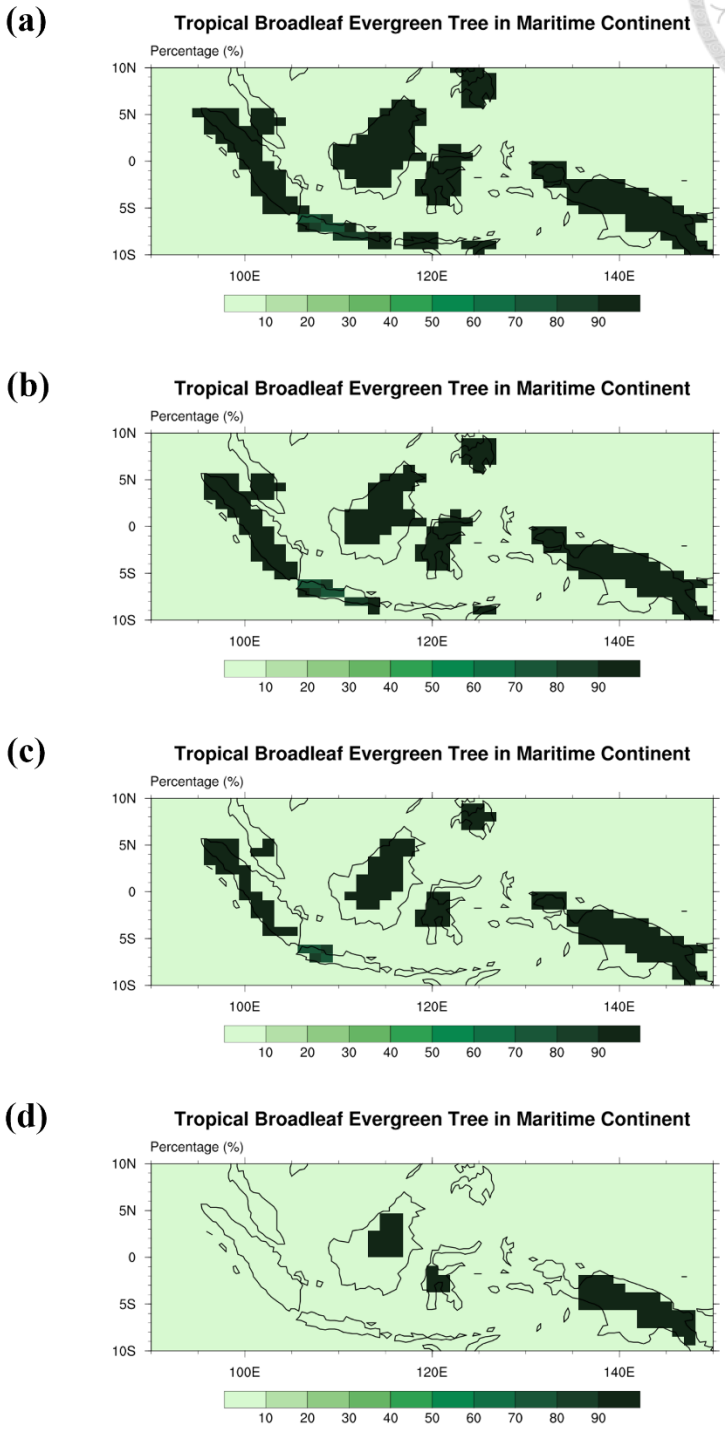

Figure 1. The forest distribution in MC region in **(a)** DEF_25、**(b)** DEF_35、**(c)** DEF_50 and **(d)** DEF_75 simulation.

doi:10.6342/NTU202303778

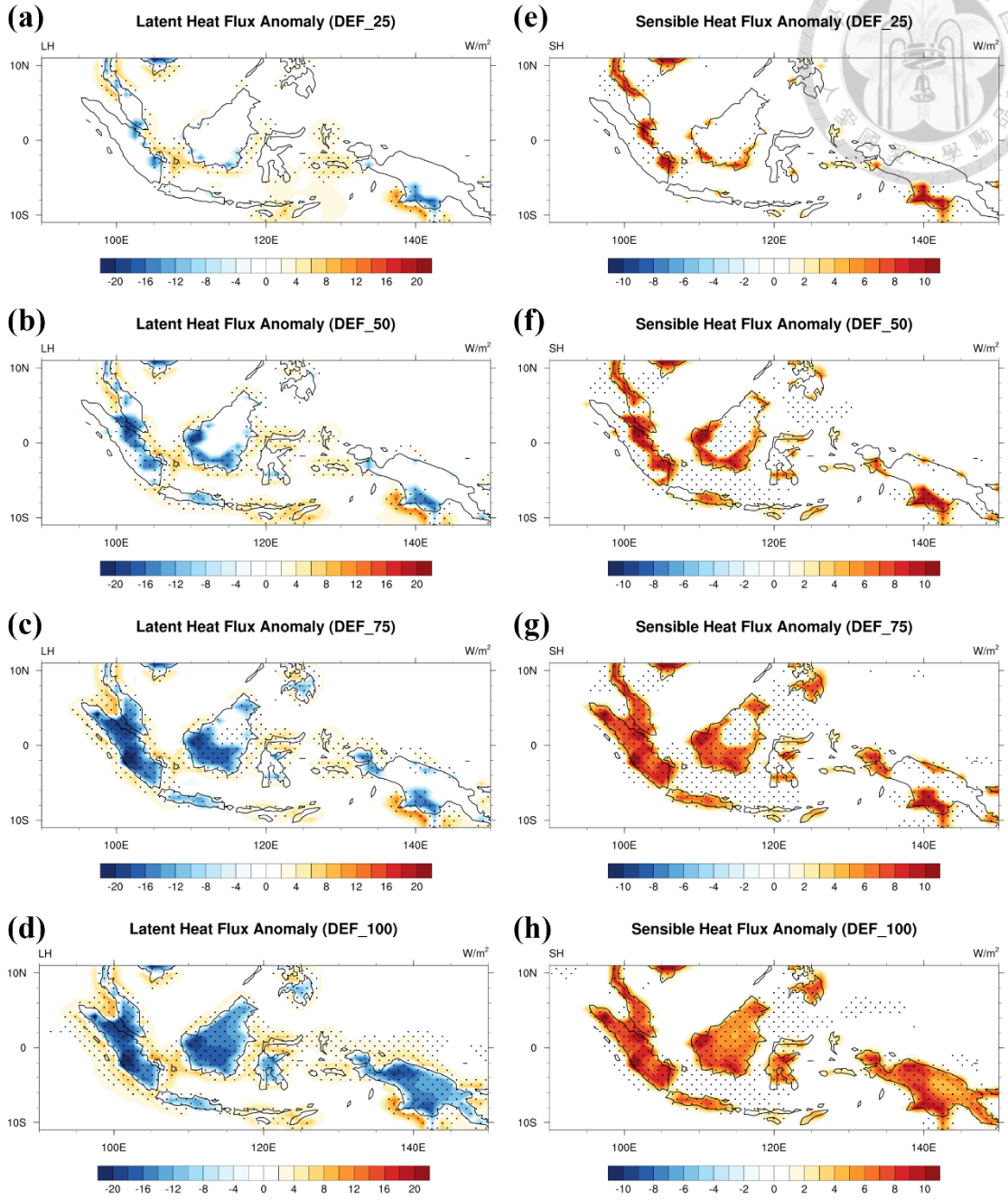

Figure 2. The spatial anomaly of **(a)** latent heat flux (DEF_25), **(b)** latent heat flux (DEF_50), **(c)** latent heat flux (DEF_75), **(d)** latent heat flux (DEF_100), **(e)** sensible heat flux (DEF_25), **(f)** sensible heat flux (DEF_50), **(g)** sensible heat flux (DEF_75), and **(h)** sensible heat flux (DEF_100). All are compared to CTR_100 and dots indicate p value<0.05.

doi:10.6342/NTU202303778

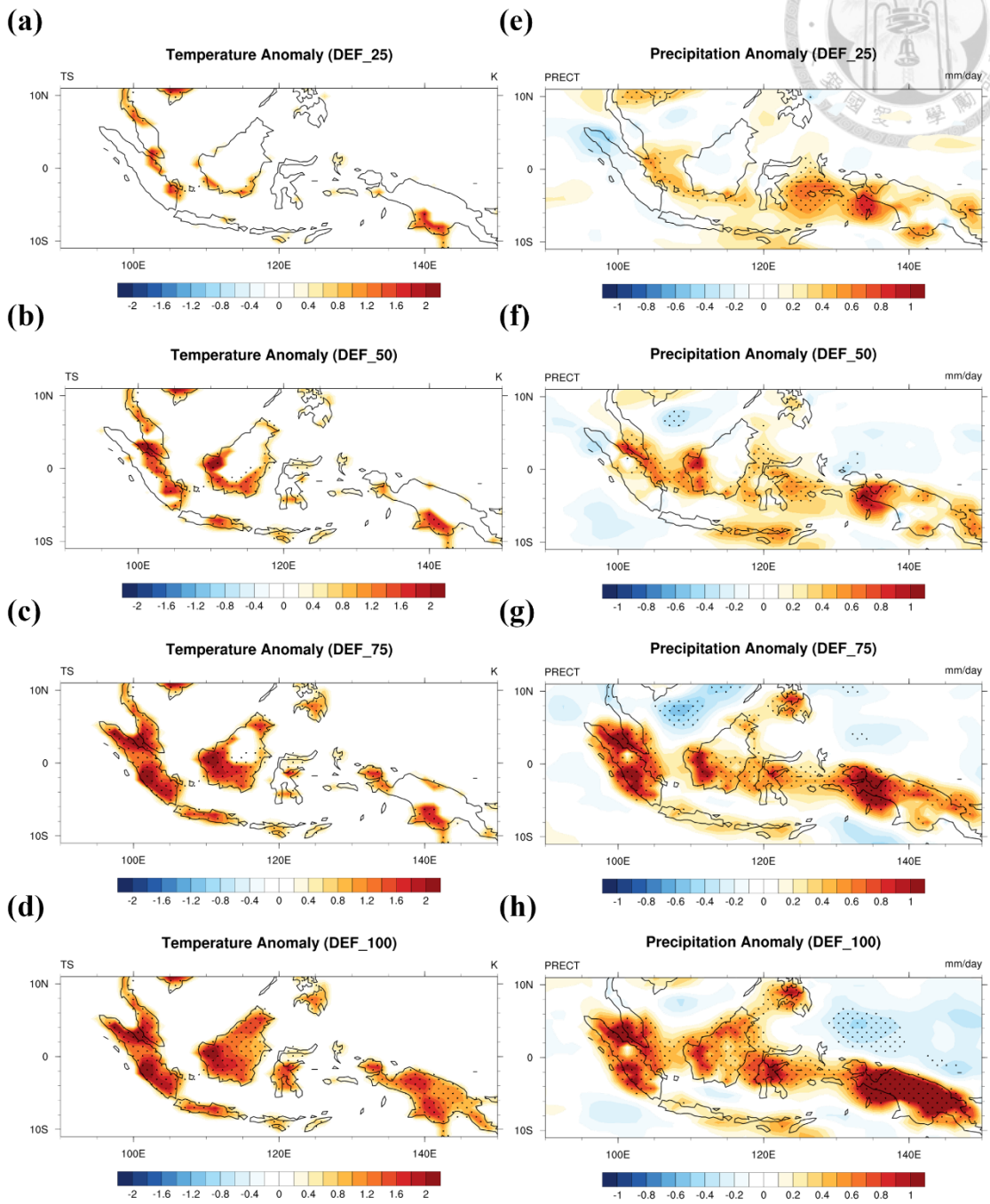

Figure 3. The spatial anomaly of **(a)** temperature (DEF_25), **(b)** temperature (DEF_50), **(c)** temperature (DEF_75), **(d)** temperature (DEF_100), **(e)** precipitation (DEF_25), **(f)** precipitation (DEF_50), **(g)** precipitation (DEF_75), and **(h)** precipitation (DEF_100). All plots are compared to CTR_100 and dotted areas indicate p value<0.05.

doi:10.6342/NTU202303778

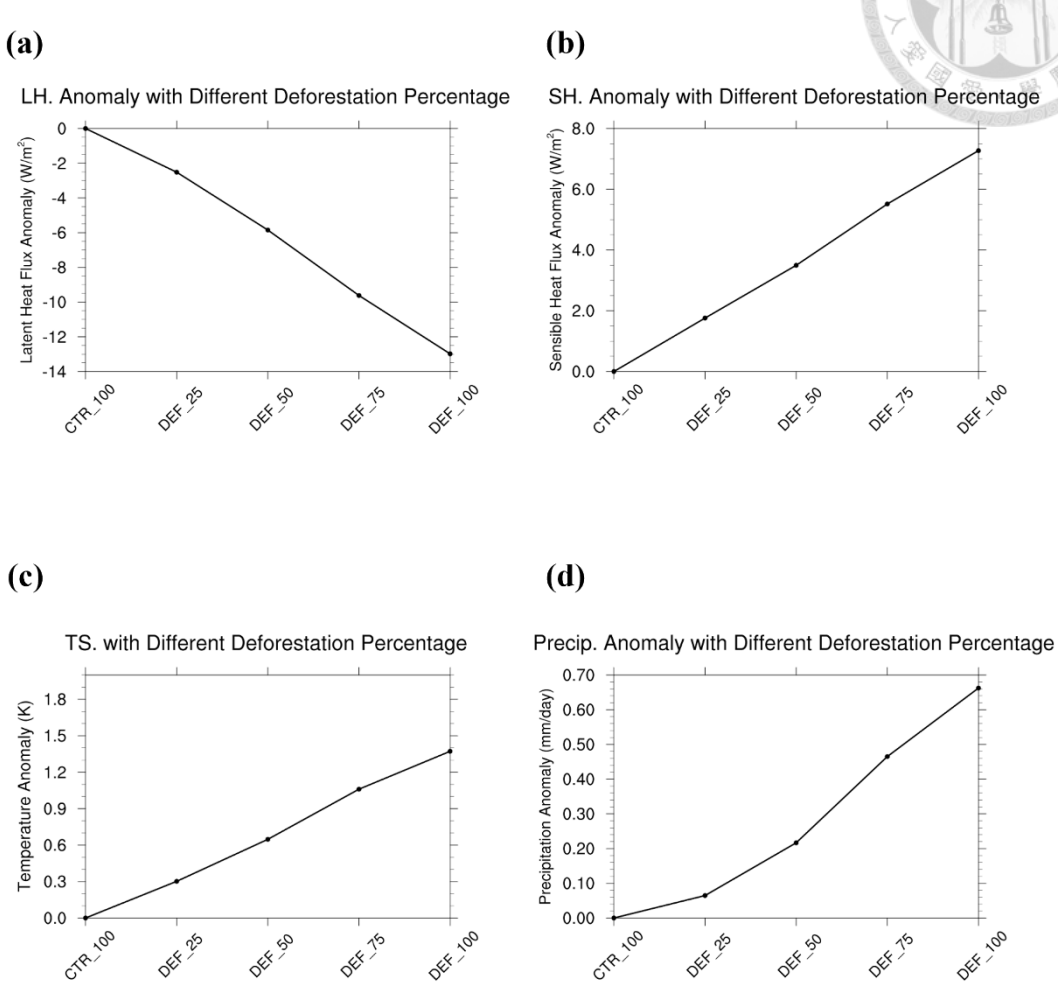

Figure 4. Annual mean **(a)** latent heat flux **(b)** sensible heat flux **(c)** surface temperature **(d)** precipitation of deforested cases compared to the control case.

doi:10.6342/NTU202303778

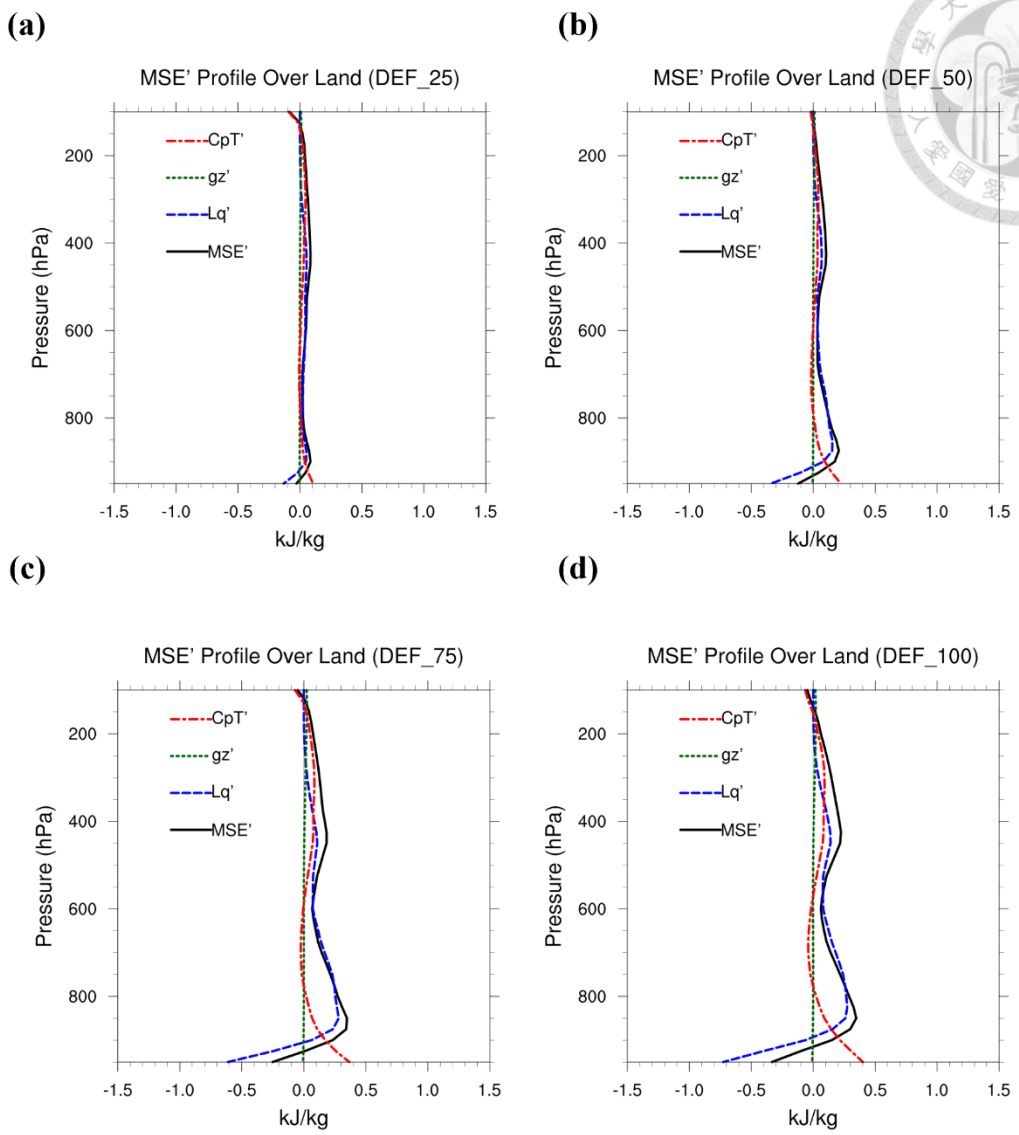

Figure 5. The anomalous MSE profile of **(a)** DEF_25, **(b)** DEF_50, **(c)** DEF_75 and **(d)** DEF_100.

doi:10.6342/NTU202303778

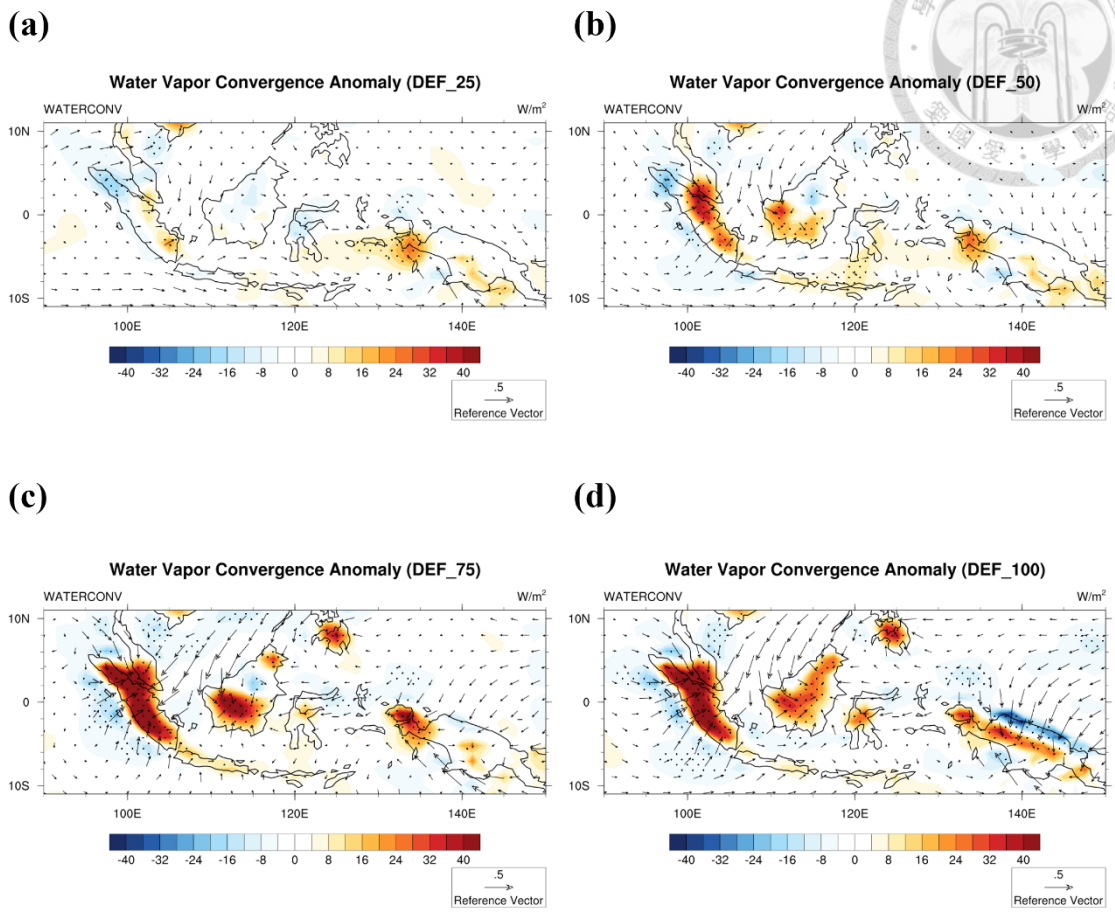

Figure 6. Annual mean of low-level moisture convergence anomaly integrated from 950 to 850 hPa with 950-hPa wind anomaly **(a)** DEF_25, **(b)** DEF_50, **(c)** DEF_75 and **(d)** DEF_100.

doi:10.6342/NTU202303778

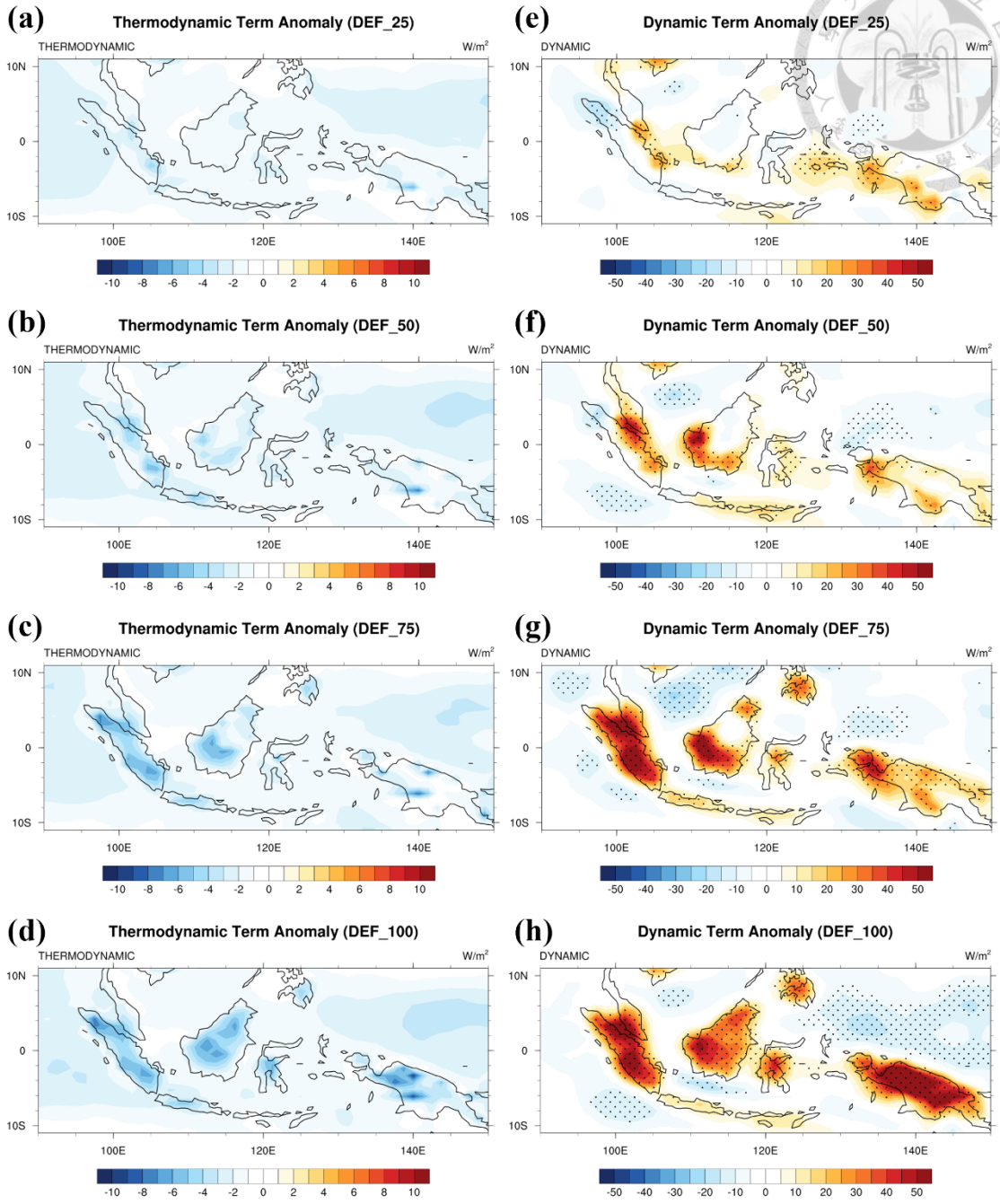

Figure 7. The spatial anomaly of **(a)** thermodynamic term (DEF_25), **(b)** thermodynamic term (DEF_50), **(c)** thermodynamic term (DEF_75), **(d)** thermodynamic term (DEF_100), **(e)** dynamic term (DEF_25), **(f)** dynamic term (DEF_50), **(g)** dynamic term (DEF_75), and **(h)** dynamic term (DEF_100). All plots are compared to CTR_100 and dotted areas indicate p value<0.05.

doi:10.6342/NTU202303778

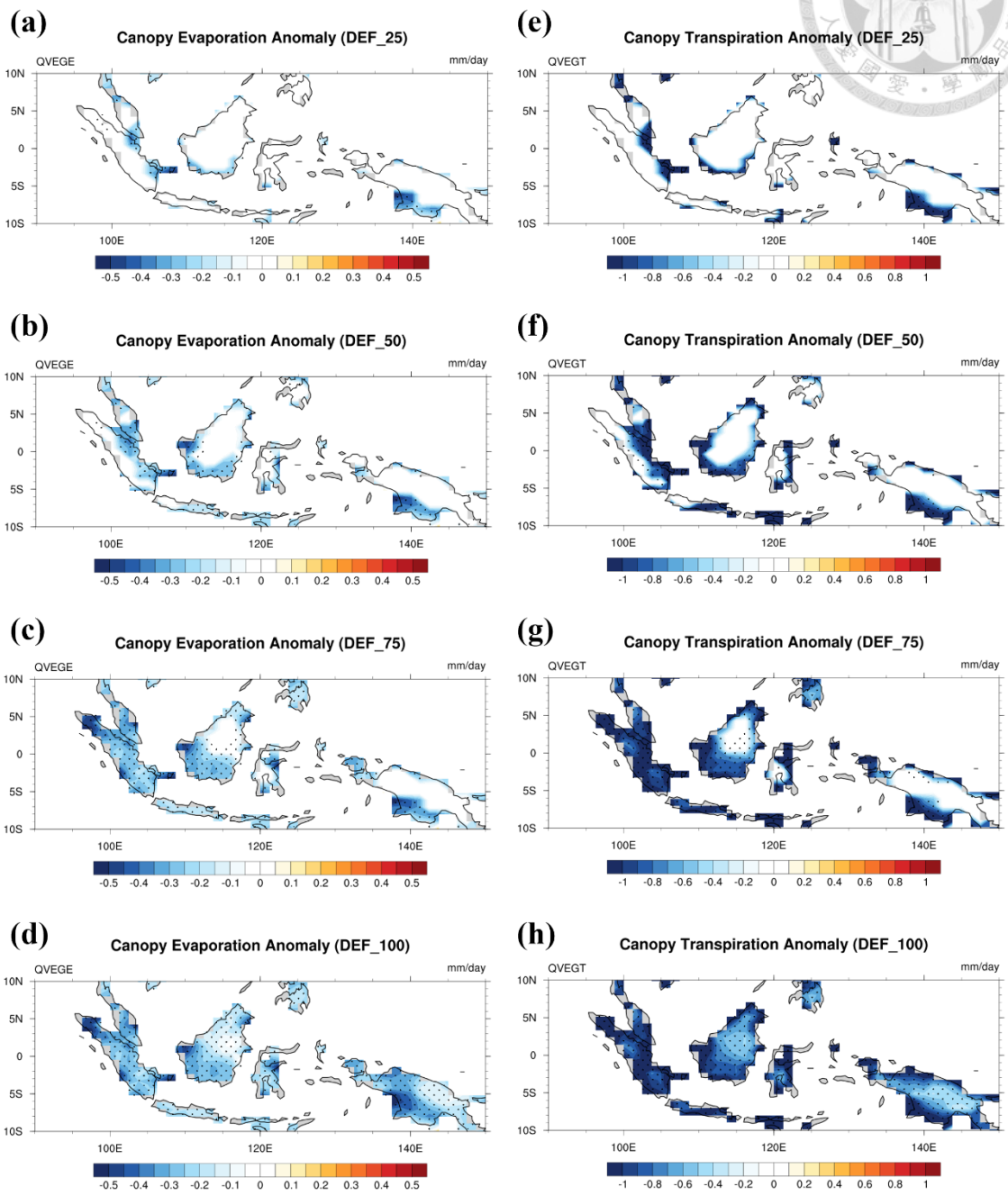

doi:10.6342/NTU202303778

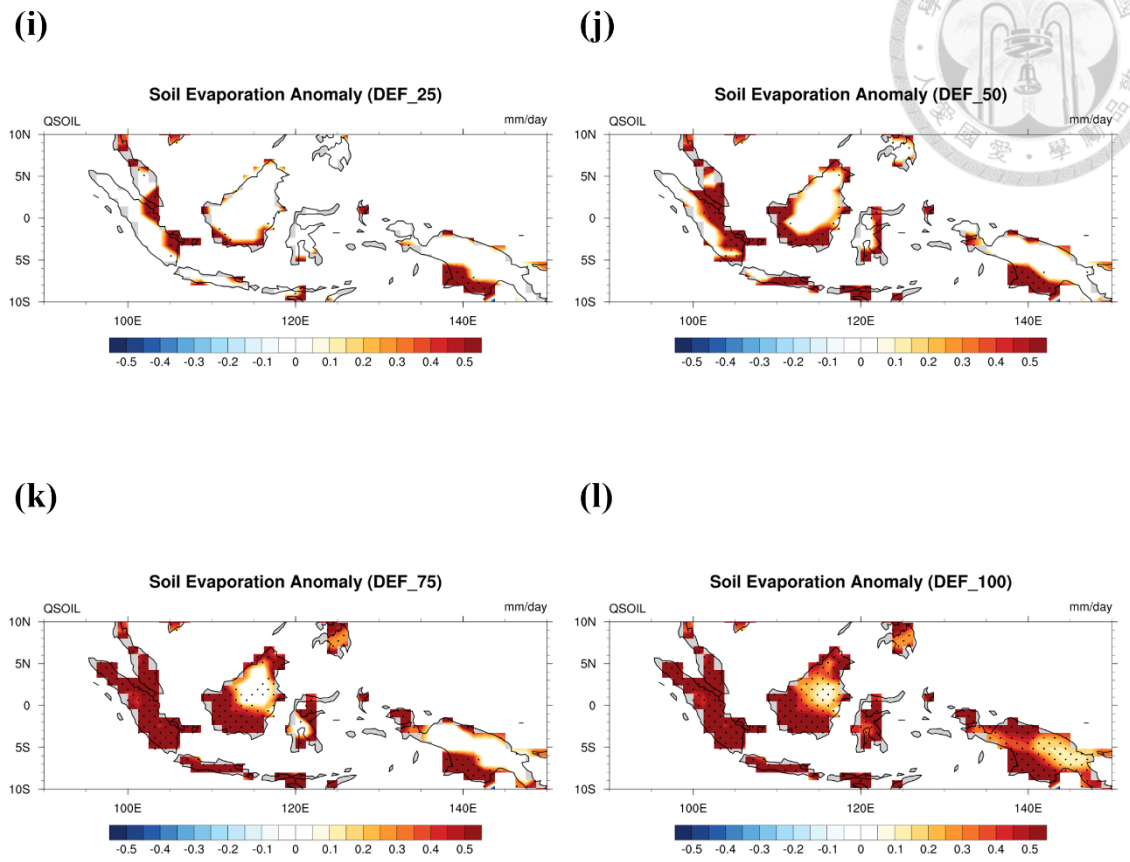

Figure 8. The spatial anomaly of **(a)** canopy evaporation (DEF_25), **(b)** canopy evaporation (DEF_50), **(c)** canopy evaporation (DEF_75), **(d)** canopy evaporation (DEF_100), **(e)** canopy transpiration (DEF_25), **(f)** canopy transpiration (DEF_50), **(g)** canopy transpiration (DEF_75), **(h)** canopy transpiration (DEF_100), **(i)** soil evaporation (DEF_25), **(j)** soil evaporation (DEF_50), **(k)** soil evaporation (DEF_75), and **(l)** soil evaporation (DEF_100). All are compared to CTR_100 and dots indicate p value<0.05.

doi:10.6342/NTU202303778

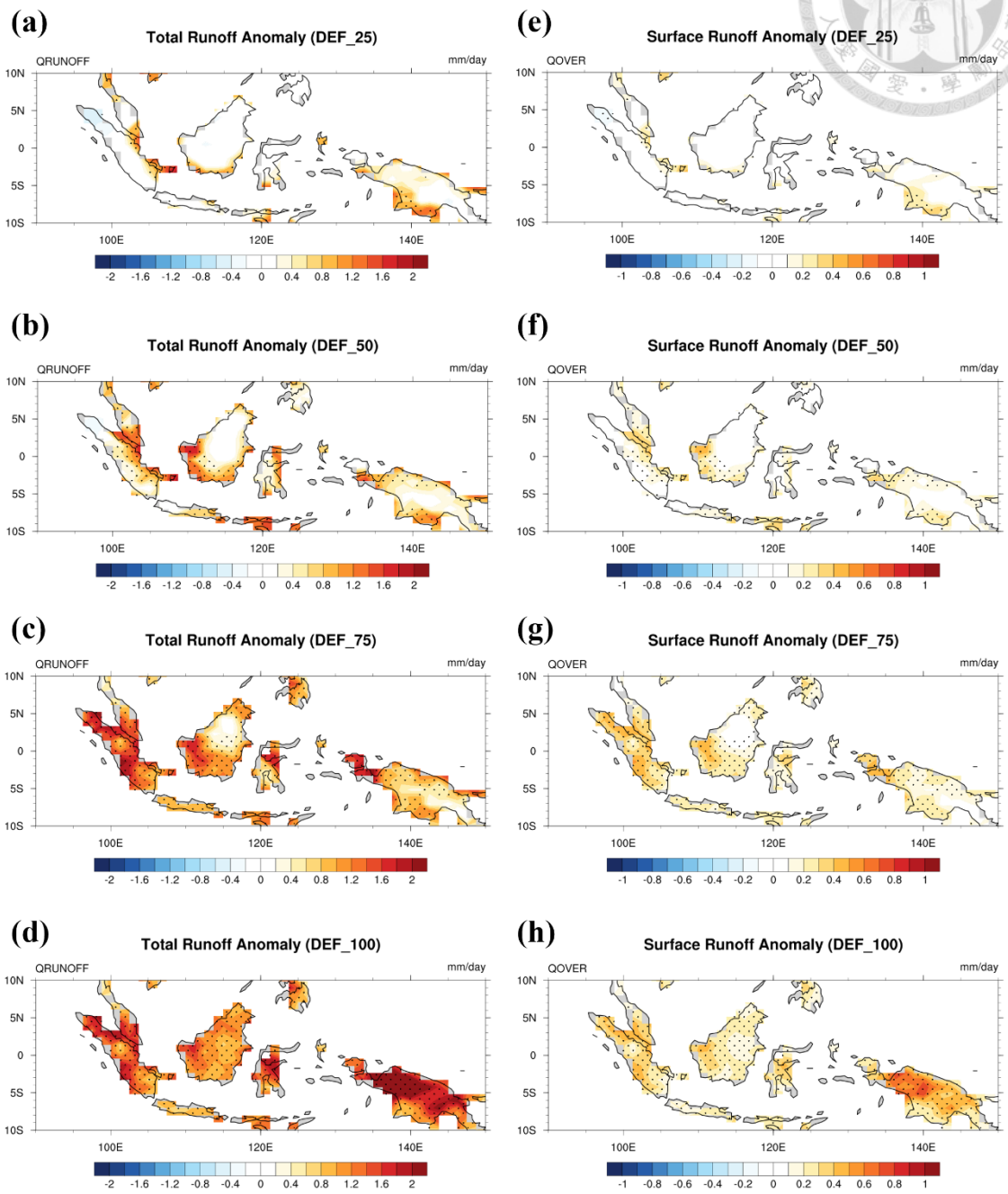

doi:10.6342/NTU202303778

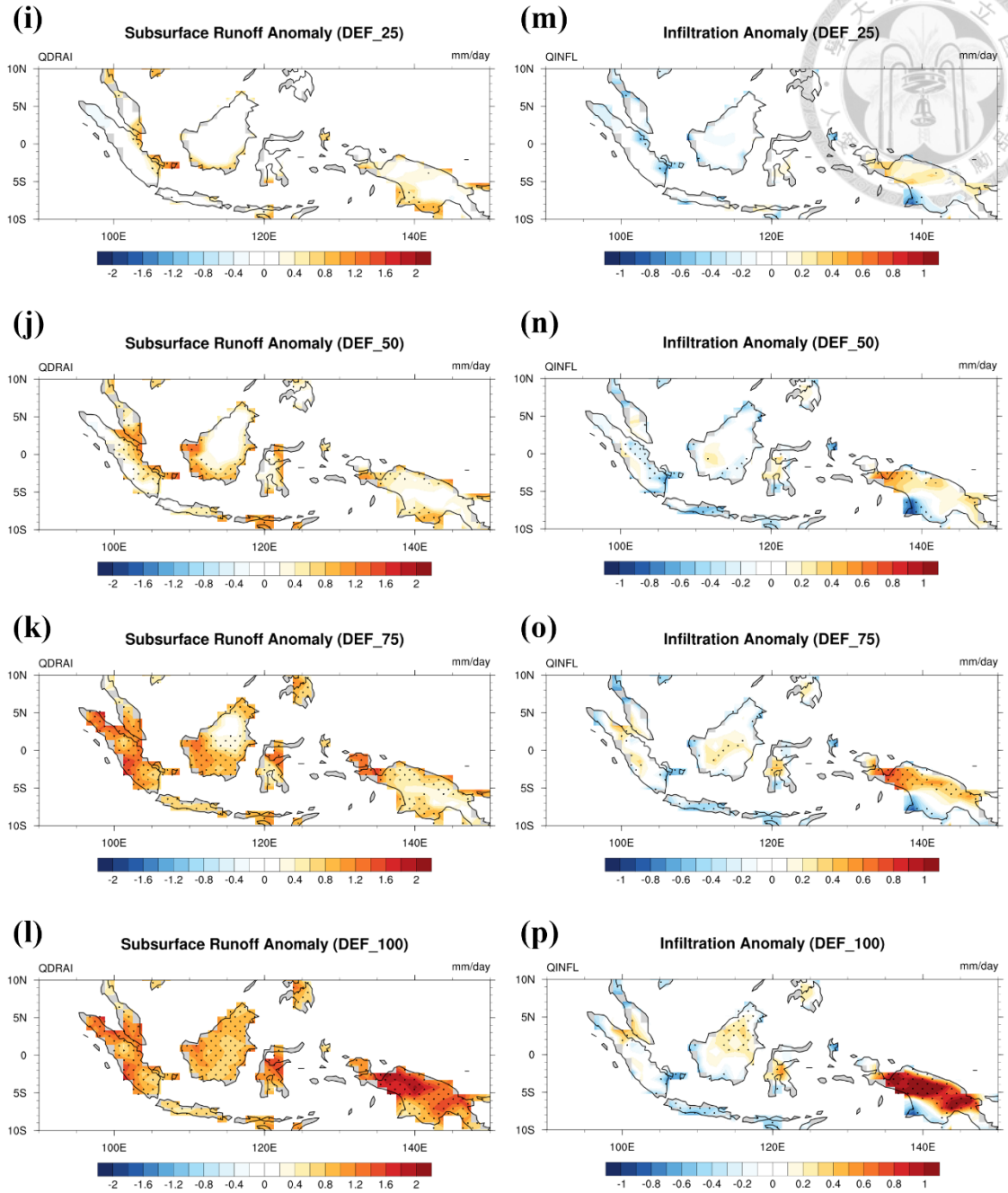

Figure 9. The spatial anomaly of **(a)** total runoff (DEF_25), **(b)** total runoff (DEF_50), **(c)** total runoff (DEF_75), **(d)** total runoff (DEF_100), **(e)** surface runoff (DEF_25), **(f)** surface runoff (DEF_50), **(g)** surface runoff (DEF_75), **(h)** surface runoff (DEF_100), **(i)** subsurface runoff (DEF_25), **(j)** subsurface runoff (DEF_50), **(k)** subsurface runoff (DEF_75), **(l)** subsurface runoff (DEF_100), **(m)** infiltration (DEF_25), **(n)** infiltration

doi:10.6342/NTU202303778

(DEF_50), **(o)** infiltration (DEF_75), and **(p)** infiltration (DEF_100). All are compared to CTR_100 and dots indicate p value<0.05.

doi:10.6342/NTU202303778

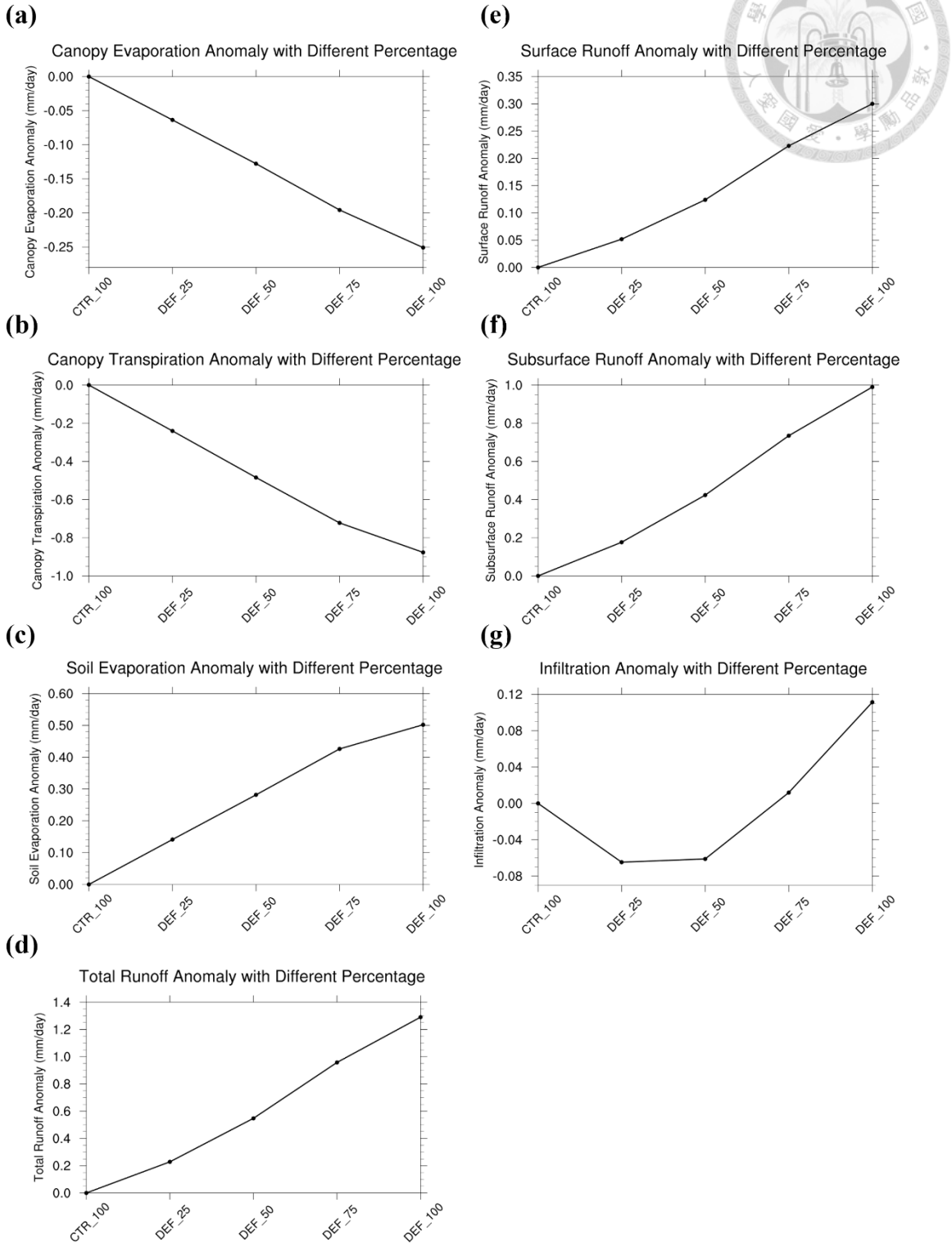

Figure 10. Annual mean **(a)** canopy evaporation, **(b)** canopy transpiration, **(c)** soil evaporation, **(d)** total runoff, **(e)** surface runoff, **(f)** subsurface runoff and **(g)** infiltration of deforested cases compared to the control case.

doi:10.6342/NTU202303778

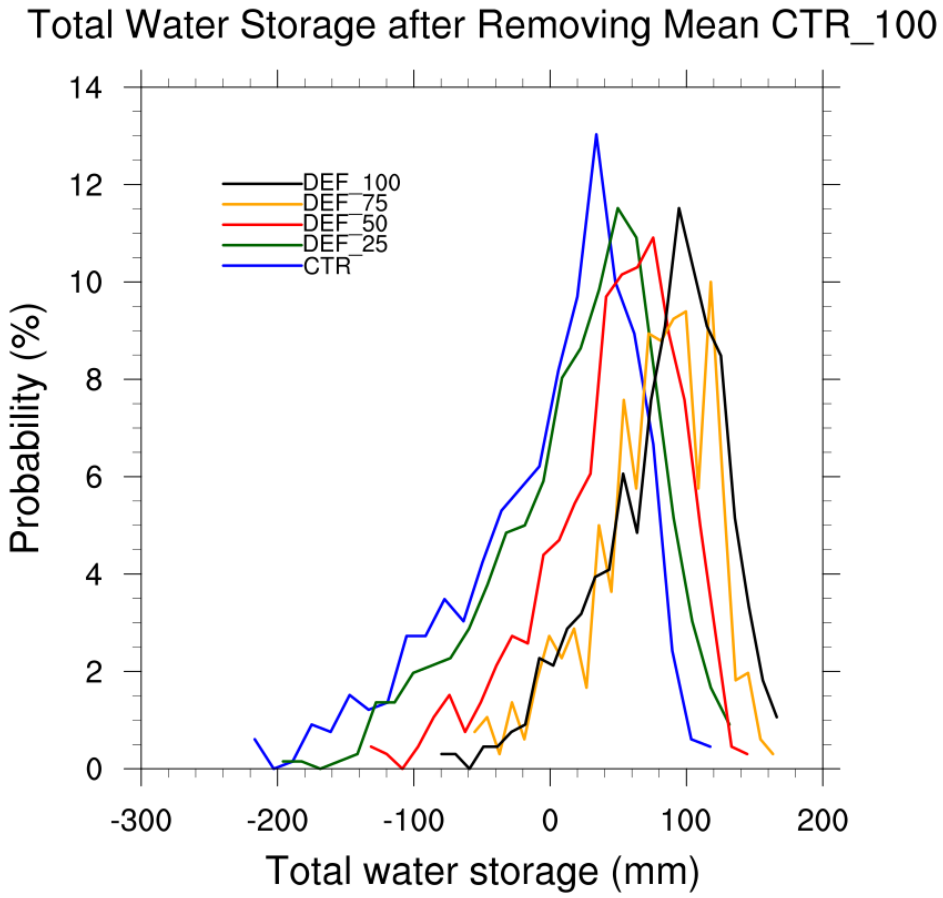

Figure 11. The probability density function of total water storage

doi:10.6342/NTU202303778

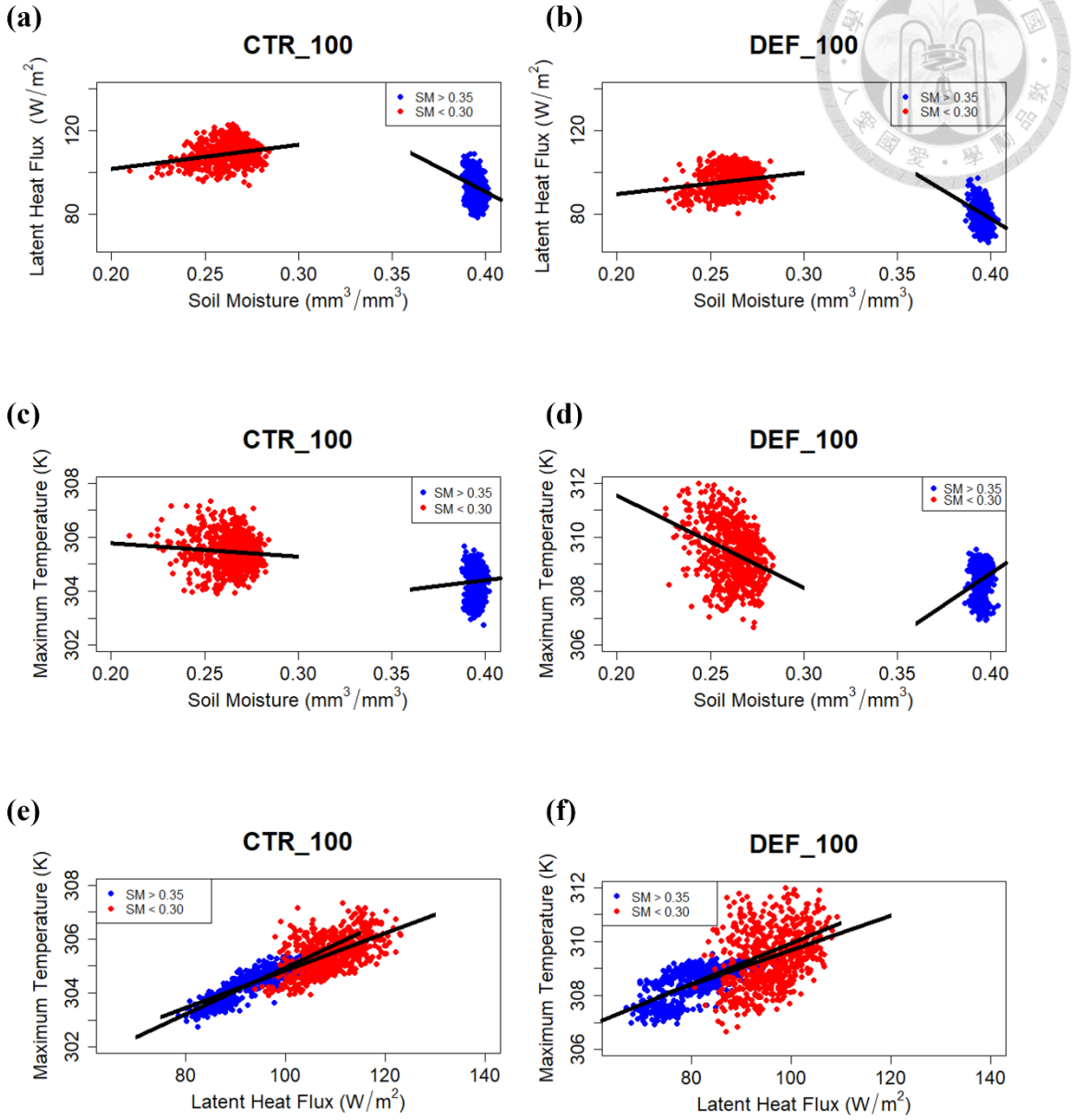

Figure 12. The scatter plot of **(a)** soil moisture and latent heat flux (CTR_100), **(b)** soil moisture and latent heat flux (DEF_100), **(c)** soil moisture and maximum temperature (CTR_100), **(d)** soil moisture and maximum temperature (DEF_100), **(e)** latent heat flux and maximum temperature (CTR_100) and **(f)** latent heat flux and maximum temperature (DEF_100).

doi:10.6342/NTU202303778

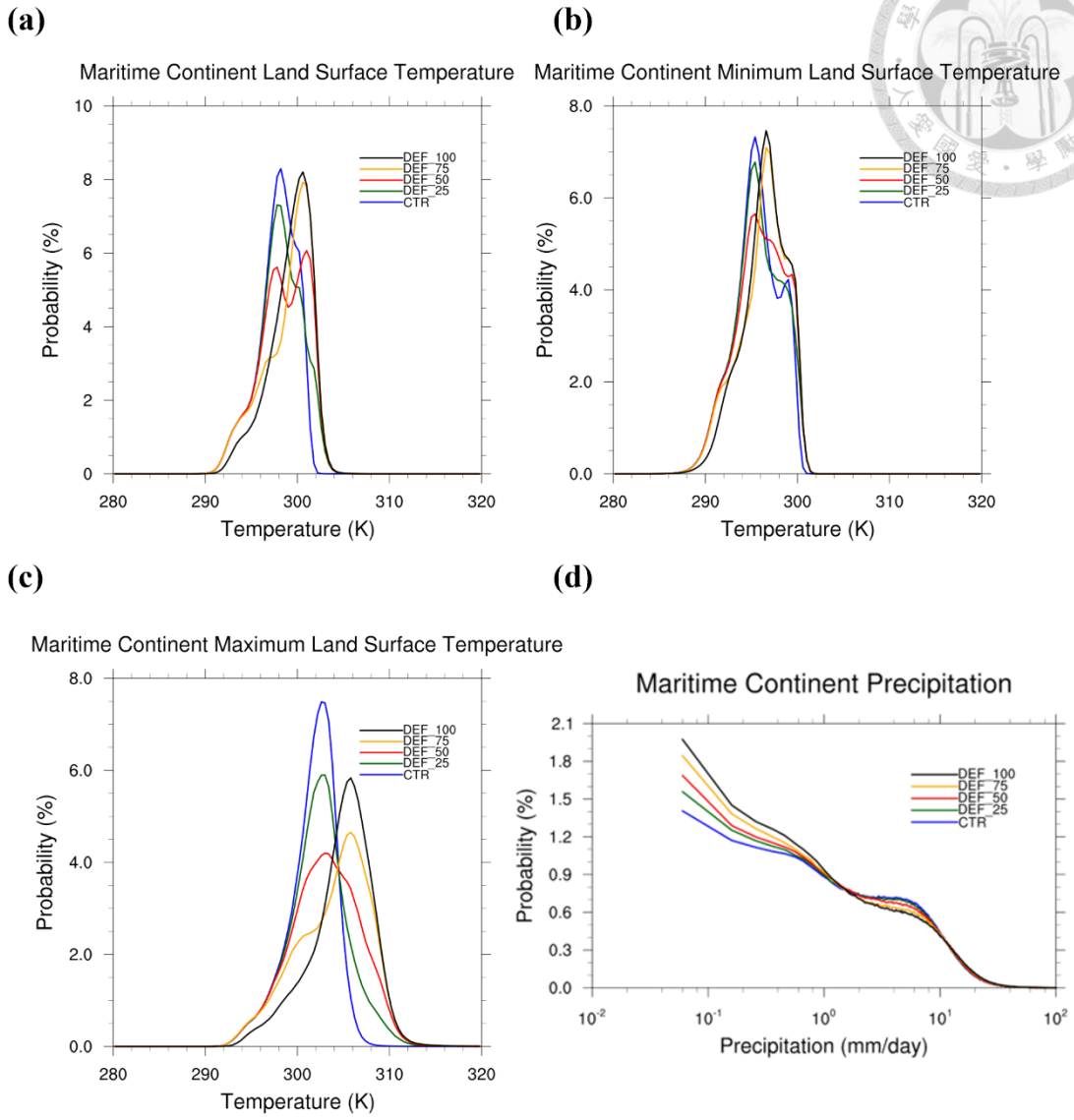

Figure 13. The probability density function of **(a)** land surface temperature, **(b)** daily minimum land surface temperature, **(c)** daily maximum land surface temperature and **(d)** land precipitation. The unit of probability is percentage (%).

doi:10.6342/NTU202303778

(a)

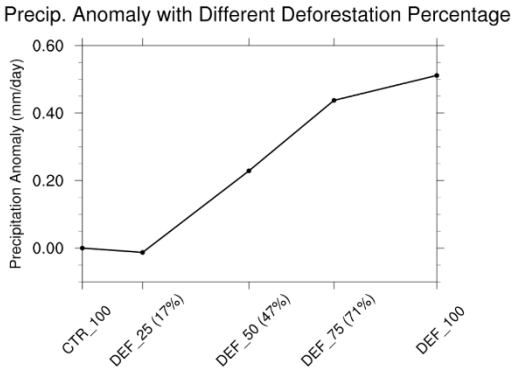

(b)

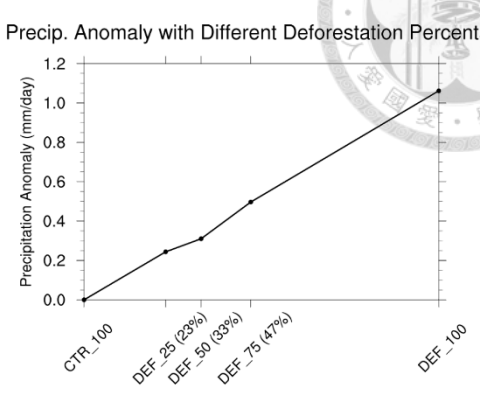

(c)

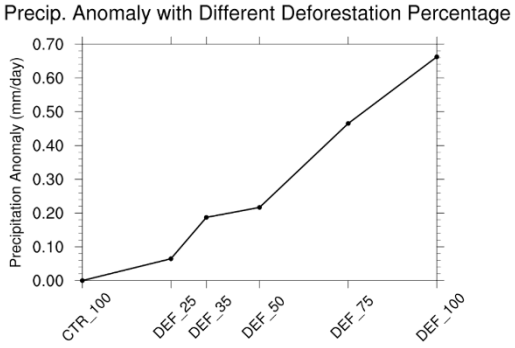

Figure 14. Annual mean precipitation for **(a)** Borneo **(b)** New Guinea and **(c)** MC region including DEF_35 compared to the control case.

doi:10.6342/NTU202303778